



Article

Surrounding Rock Deformation Mechanism and Control Technology for the Roadway in the Fault-Disturbed Zone under Special-Shaped Coal Pillars

Chao Liu ^{1,2}, Fangtian Wang ^{1,2,*}, Zhenyu Zhang ³ , Dongxu Zhu ⁴, Wenhua Hao ^{1,2}, Tiankuo Tang ^{1,2}, Xutong Zhang ^{1,2}  and Chenguang Zhu ⁴

¹ School of Mines, China University of Mining and Technology, Xuzhou 221116, China; liuc1116@163.com (C.L.); 15695253155@163.com (W.H.); tiankuo1124@163.com (T.T.); ts22020228p21@cumt.edu.cn (X.Z.)

² State Key Laboratory of Coal Resources and Safe Mining (CUMT), Xuzhou 221116, China

³ State Key Laboratory of Coal Mine Disaster Dynamics and Control, Chongqing University, Chongqing 400044, China; zyzhang@cqu.edu.cn

⁴ Luwa Coal Mine, Shandong Lutai Holding Group, Jining 272350, China; zhudongxu11@163.com (D.Z.); 15619020771@163.com (C.Z.)

* Correspondence: wangfangtian111@163.com

Abstract: In order to explore the impact of residual special-shaped coal pillars and fault disturbances on the lower layered roadway, this study takes the short-distance coal seam mining in Luwa Coal Mine as the engineering background to explore the surrounding rock deformation mechanism along the mining roadway in the fault-disturbed zone under special-shaped coal pillars, it presents the roadway surrounding rock control technology and it conducts on-site industrial test verification. The study shows that the abutment pressures on the floor of special-shaped coal pillars are distributed as “three peaks and two ridges”. The part beneath coal pillars is mainly disturbed by vertical stresses, while the part below the coal pillar edge is co-affected by vertical stresses and shearing stresses, generating a stress concentration coefficient ranging from 1.26 to 1.38 in the lower coal seam. According to the superposed effects of special-shaped coal pillars and fault disturbance on the mining roadway, the mining roadway is divided into the lower section of goaf, the section crossing the coal pillar edge, the lower section of coal pillars, and the section obliquely crossing the coal pillar edge. According to the above sections, the segmental control strategies of “improving stress distribution on surrounding rock + reinforcing support on special sections” are proposed. A joint control technology of large-diameter drilling hole pressure relief and special section anchor cable reinforcement support was adopted to carry out on-site industrial testing and monitoring. Overall, the convergence rate on the roadway surrounding rock is controlled within 5%, and the deformation of roadway surrounding rock is under effective control.

Keywords: short-distance coal seams; special-shaped coal pillar; fault structure; abutment pressure; segmental control



Citation: Liu, C.; Wang, F.; Zhang, Z.; Zhu, D.; Hao, W.; Tang, T.; Zhang, X.; Zhu, C. Surrounding Rock Deformation Mechanism and Control Technology for the Roadway in the Fault-Disturbed Zone under Special-Shaped Coal Pillars. *Processes* **2023**, *11*, 3264. <https://doi.org/10.3390/pr11123264>

Academic Editors: Junwen Zhang, Xuejie Deng, Zhaohui Wang and Carlos Sierra Fernández

Received: 3 October 2023

Revised: 8 November 2023

Accepted: 15 November 2023

Published: 22 November 2023



Copyright: © 2023 by the authors. Licensee MDPI, Basel, Switzerland. This article is an open access article distributed under the terms and conditions of the Creative Commons Attribution (CC BY) license (<https://creativecommons.org/licenses/by/4.0/>).

1. Introduction

China has complex conditions for coal occurrence. Short-distance coal seams are widely distributed in China’s coalfields. In the mining of short-distance coal seams, there are often coal pillars protecting roadway sections that remain after overlying strata are mined. If fault structure and other factors exist, the mining working face will become irregular. Then, special-shaped coal pillars protecting roadway sections will remain between adjacent working faces. After the upper layer working face is mined, the stresses are redistributed on lower layer surrounding rock. Under superposed irregular stresses, the mining roadway in the lower coal seam will easily have problems, such as roof fracture development, stress concentration, and large deformation [1–5].

A large number of studies have been made on the influence of remaining coal pillars in the mining of short-distance coal seams on the stability of mining roadway. Hu et al. [6] analyzed the relationship between the internal stress change rate in the lower coal seam and the sizes of remaining coal pillars in the upper coal seam, and they proposed measures to ensure the mining of lower coal seams and roadway maintenance. Li et al. [7] studied the disturbance evolution mechanism of coal pillars in the remaining sections on the overlying strata to floor stresses before and after the mining of underlying coal seams by means of field measurement and theoretical analysis. Wang et al. [8] established a numerical calculation model of mining stress response in the final mining section of the working face and studied the superposed effects of advanced abutment pressure in the working face during mining disturbance, as well as the stress evolution and cumulative damage mechanism of coal pillars along the roadway under gradual loading conditions. Wang et al. [9] identified the stress-concentrated area in the floor through the maximum principal stress concentration coefficient, studied the evolution characteristics of the stress-concentrated area in the floor at different mining stages, and regarded a staggered distance of 10–15 m between coal pillar and roadway as the optimal internal. Du and Huang [10] used physical similarity simulation and numerical simulation methods to systematically study the structural evolution law of “goaf—remaining coal pillars—mining roadway” in the mining of short-distance coal seams. Then, they applied the continuous damage model to study the damage and fracture law in the main roof between short-distance coal seams and obtained the length calculation formula for initial fracture in the damaged main roof. Wang et al. [11] applied FLAC3D to establish a numerical calculation model of the dynamic damage of the coal pillar dam under a complex stress field, and they pointed out the distribution of lateral abutment pressures in the mining of multiple working faces and the dynamic response law of the coal pillar dam under a dynamic load.

The existence of a fault in the structural plane destroys the continuity of the stratum. Mining near the fault is more prone to mine dynamic disasters. Ji et al. [12] used numerical stimulation calculation to obtain the stress change characteristics when the lower working face of the fault is parallel to and perpendicular to the fault. Duan et al. [13] conducted a triaxial compression test by simulating intact rock sample presegmentation to the fault, by which they studied the connection between the maximum principal stress and the fault plane direction. Sainoki and Mitri [14] adopted dynamic numerical simulation to analyze that the maximum shearing displacement in the fault caused by mining is related with fault dip, mining depth and other factors. Feng et al. [15,16] analyzed the rockburst response induced by the mining effect and structural plane effect for a deep-buried tunnel, and they proposed the principles, design methods and basic ideas of the energy-release support system. Wang et al. [17] used laboratory experiments to study the influence of fault shape on the stress field of roadway surrounding rock, and they claimed that fault dip is a key factor that influences unstable surrounding rock in the roadway.

The existing research results focus on the layout of roadway under regular coal pillars for short-distance coal seams and the study of coal seams [18]. However, when it is difficult to reserve coal pillars protecting the roadway in regular sections and it is necessary to arrange the roadway and mine the coal seam under the fault's influence, it is urgently necessary to further discuss the stress disturbance degree, influence range, and strata behaviors of special-shaped coal pillars and fault disturbance area on the mining roadway. This study takes Shandong Luwa Coal Mine as the engineering background and establishes theoretical models of support pressure for special-shaped coal pillars and fault disturbance. Numerical simulation methods are used to study the superimposed effects of residual special-shaped coal pillars and fault disturbance on the stress environment of mining roadway. Therefore, we will explore measures to control the stability of roadway surrounding rock when it passes through the remaining special-shaped coal pillars in the fault disturbance zone during close-range coal seam mining. By monitoring the deformation of the roadway surrounding rock, the rationality of support optimization is verified, providing a scientific basis for the design of tunnel support under similar conditions.

2. Engineering Background

In the third mining area of Luwa Coal Mine, the principal coal seams are the 3_{upper} and 3_{lower} coal seams in the middle of Shanxi Team. The thickness of the 3_{upper} coal seam is 1.2–2.4 m, and the average coal thickness is 2.04 m. The dip angle of the coal seam is $0\text{--}10^\circ$, with an average of 6° . The coal seam has a simple structure and relatively stable thickness, mainly consisting of bright coal. The thickness of the 3_{lower} coal seam is 2.79–5.14 m, and the average coal thickness is 3.79 m. Coal seam occurrence: $305\text{--}315^\circ$, $\angle 0\text{--}10^\circ$, average 6° . The average distance between the 3_{upper} coal seam and the 3_{lower} coal seam is about 30 m. The $33_{\text{upper}}01$ working face and the $33_{\text{upper}}03$ working face are two adjacent working faces in the 3_{upper} coal seam, and they were mined successively. Influenced by DF87 fault, the two working faces are irregularly arranged on contracted faces in different positions, where special-shaped coal pillars remain. The DF87 fault is a normal fault with an NE strike, SE dip, a 70° dip angle, and a 0–15 m drop. The spatial position relationship between the upper and lower working faces is shown in Figure 1.

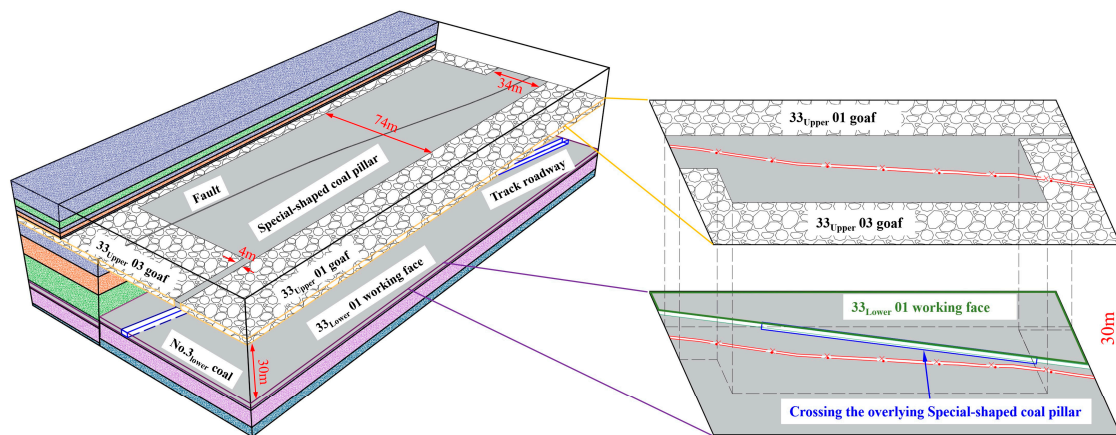


Figure 1. Spatial position relationship between the working faces.

The $33_{\text{lower}}01$ working face is located below the two goafs. Influenced by the fault, the track roadway on the $33_{\text{lower}}01$ working face crosses the lower part of remaining overlying special-shaped coal pillars during the excavation process. The roadway section, rectangular in shape, has a net width of 4 m, a net height of 2.6 m, and a net section of 10.4 m^2 .

The roadway is supported by a combination of anchor cable, bolt and metal mesh; the roof is supported by “bolt + anchor cable + metal mesh”. The rock bolt is in a resin deformed steel bar, with a strength of No. 5 (A5) steel, a size of $\Phi 20 \times 2000\text{ mm}$, and a row spacing of $1000 \times 1000\text{ mm}$. The anchor cable is a $\Phi 17.8 \times 6000\text{ mm}$ steel strand. One steel strand is arranged in each row, with a row-to-row distance of 3000 mm . The whole fault is covered by 10# iron wire diamond mesh of $5000 \times 800\text{ mm}$, and the mesh size is $75 \times 75\text{ mm}$. The two sidewalls are supported by “bolt + metal mesh”; the bottom angles are supported by “inclined bolts”. The rock bolt is $\Phi 18 \times 1800\text{ mm}$ of full-threaded FRP resin, with a row spacing of $1000 \times 1000\text{ mm}$.

After the mining in the working face of the upper slice, the coal pillars protecting the roadway changed into remaining coal pillars, and the coal pillar stresses were re-distributed. When the support stress of the coal pillar bottom plate is transmitted to the lower layer, it will change the stress environment of the lower layer coal seam. Influenced by the stress environment and mining of surrounding rock, the ground pressure on special sections in the $33_{\text{lower}}01$ track roadway appeared to be severe [19,20], as shown in Figure 2. The main characteristics are as follow:

- (1) Under the superposed effects of special-shaped coal pillars and fault disturbance, some key areas in the roadway were deformed greatly after mining. The roof bent and sank. Some of it was pressed and destroyed, resulting in partial collapse and broken pieces.

- (2) The roadway sidewalls bulged, and the bolts at sidewall corners sank in. Occasionally, small rocks slid from sidewalls, forming a string bag.
- (3) The rock bolt (cable) supporting components failed. Influenced by highly irregular abutment pressure, the failed part of the rock bolt (cable) in the roadway direction was obviously irregular. There was obvious concave deformation in the rock bolt (cable) tray.

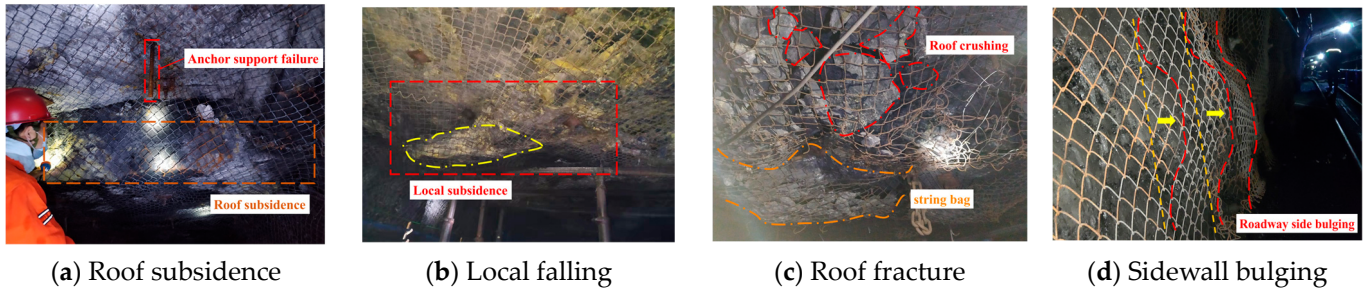


Figure 2. Deformation characteristics of surrounding rock in the 33_{lower}01 track roadway.

In order to accurately grasp the mechanical properties of the top and bottom rock layers in the 33_{lower} 01 track roadway, after drilling and coring, one must determine the required rock sample size and quantity according to different rock types and measurement methods, as well as process, classify, and mark them, as shown in Figure 3.

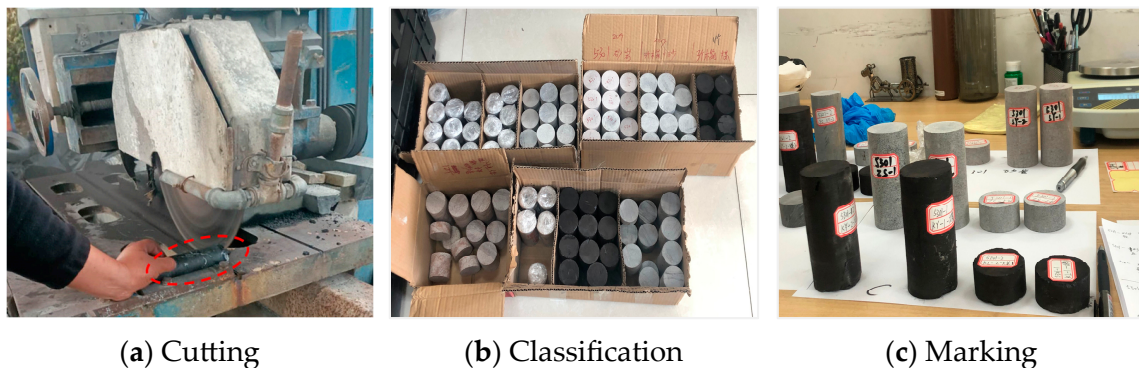


Figure 3. Coal and rock sample processing.

Conduct laboratory physical and mechanical parameter tests on the selected rock core, using uniaxial compression, uniaxial tensile, and shear tests, respectively, and adopt $\varnothing 50 \times 100$ mm, $\varnothing 50 \times 25$ mm, $\varnothing 50 \times 50$ mm (standard sample). The experimental process is shown in Figure 4, and the comprehensive histogram, physical and mechanical parameters are shown in Figure 5. The experimental process strictly followed the “Regulation for testing the physical and mechanical properties of rock (DZ/T0276.1-2015~DZ/T0276.31-2015)”, and the experimental results show that the coal lithology is relatively soft, and the arithmetic mean compressive strength is 6.94 MPa. Under the action of vertical support pressure, the horizontal deformation is relatively large. The direct roof is mudstone, with an arithmetic mean compressive strength of 20.99 Mpa. The rock is relatively soft, with weak bearing capacity and deformation resistance and poor mechanical properties. Therefore, the roof needs to be strengthened in management to prevent direct roof collapse. The basic roof is medium sandstone, with an arithmetic mean compressive strength of 64.01 Mpa. The compressive strength is high and not easy to break. Under the action of bearing pressure, it is not easy to break and deform, and it has strong anti-interference ability.

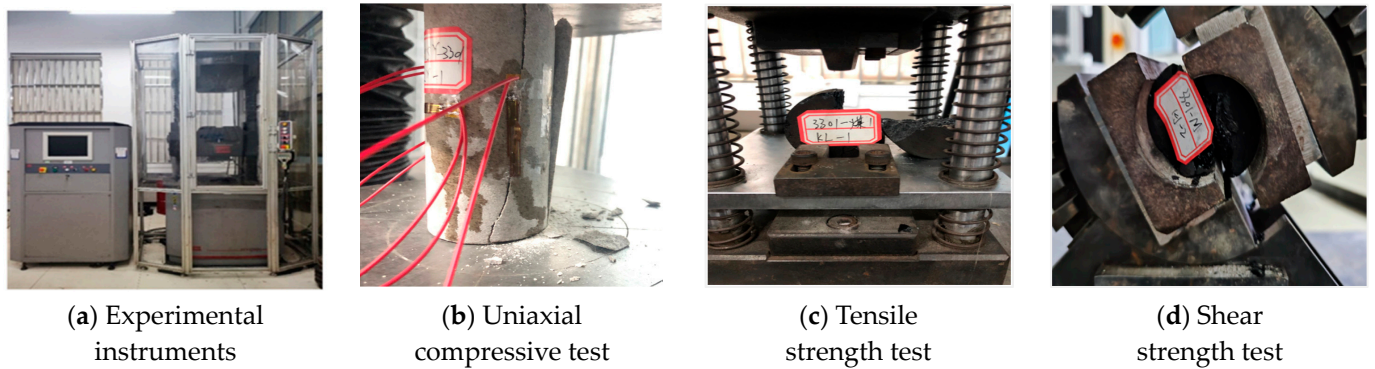


Figure 4. Mechanical parameter experiment.

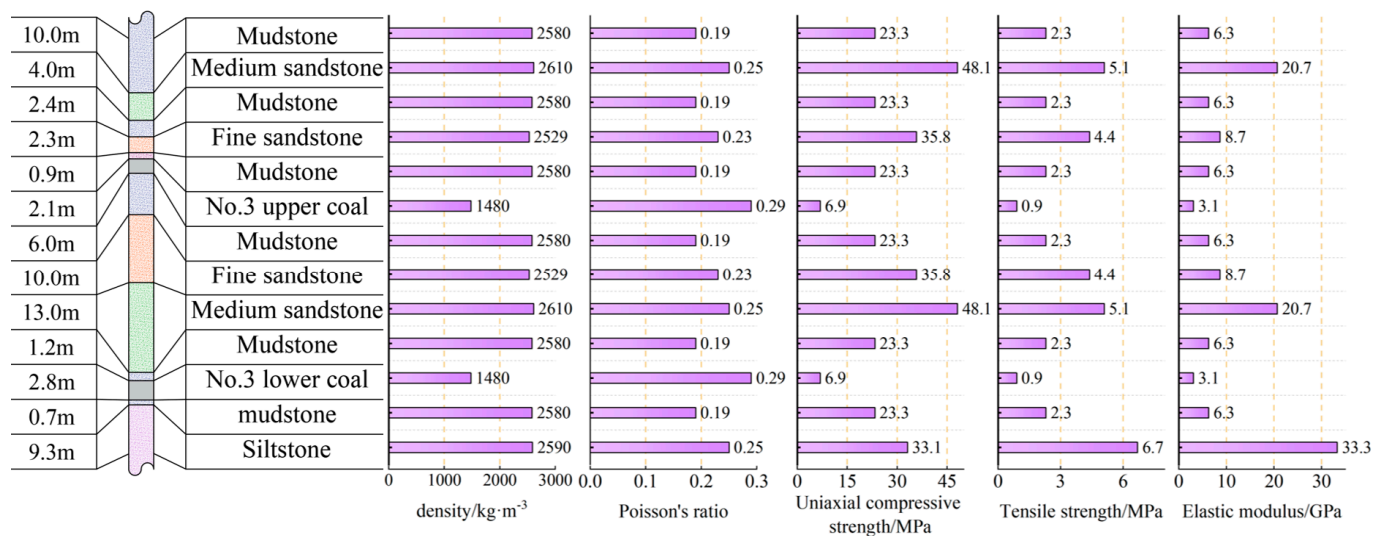


Figure 5. Comprehensive histogram.

3. Superposed Effects of Special-Shaped Coal Pillars and Fault Disturbance

3.1. Stress Distribution Characteristics in the Floor of Special-Shaped Coal Pillars

As the 33_{upper01} working face and 33_{upper03} working face were mined successively, the coal pillars protecting roadway sections changed into remaining coal pillars. The coal pillars were influenced by the cantilever structure of the goaf and the self-weight stress in the overlying strata, and the stress distribution state changed greatly and the stresses were distributed according to certain laws [21,22]. The distribution of abutment pressures in coal pillars varies with the coal pillar width. When the coal pillar is small, such as the coal pillar in Section C-C, which is only 4 m wide, it is seriously broken and relieves pressure influenced by the mining of working faces on both sides. At this moment, both the vertical stress and horizontal stress in the coal pillar are less than the initial rock stress [23]. The stress distributions in Section A-A and Section B-B are both bimodal, and Section A-A is more prone to the superposed effects of concentrated stresses on both sides. As shown in Figure 6, the stress distributions in different sections of special-shaped coal pillars are analyzed, taking the abutment pressure distribution on one side of the coal pillar as the triangular load from the coal wall to the peak stress and the trapezoidal load from the peak stress to the initial rock stress.

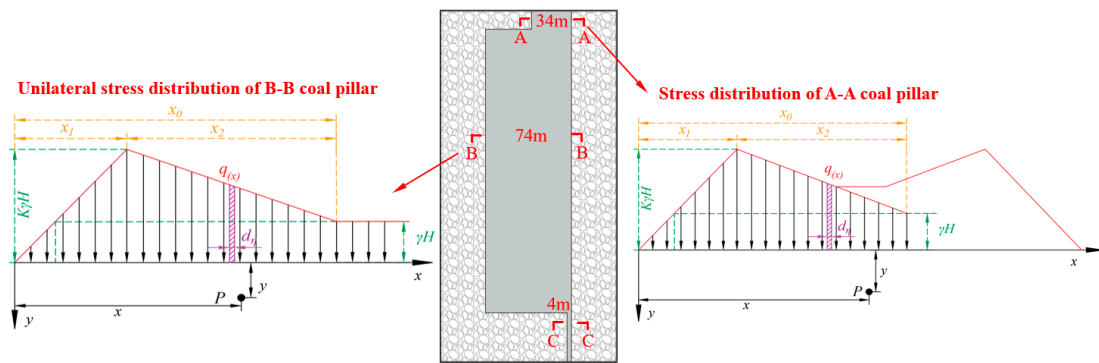


Figure 6. Distribution model of abutment pressures in different sections of special-shaped coal pillars.

When the coal pillar is stressed stably, there is the decompression zone, the pressurization zone, and the pressure stabilization zone from the edge to the depth of the coal pillar. The stress distribution state represents the damage and failure process of the coal pillar. The farther the coal body is from the physical coal edge, the stronger the bearing capacity. According to the characteristics of physical coal deformation and stress distribution, the part from the edge to the depth of the coal pillar is divided into the abutment pressure influence zone x_0 (the limit equilibrium zone x_1 , the elasticity zone x_2) and the initial stress zone [24,25]. The stress state at any point in the front of the free coal sidewall can be taken as the stress solution under the concentrated load of the semi-infinite elastic body. If the concentrated stress peak is taken, k is the stress concentration coefficient, and γH is the initial rock stress. The load $q(x)$ is:

$$q(x) = \begin{cases} \frac{k\gamma Hx}{x_1} & x \in [0, x_1] \\ \gamma H \left[\frac{(1-k)(x-x_1)}{x_0-x_1} + k \right] & x \in [x_1, x_2] \end{cases} \quad (1)$$

where $x = \eta$, the differential line segment $d\eta$ is taken, then the stress component when $qd\eta$ is at $P(x,y)$ in this differential line segment is:

$$\begin{aligned} d\sigma_y &= -\frac{2q(\eta)d\eta}{\pi} \frac{y^3}{[(x-\eta)^2+y^2]^2} \\ d\sigma_x &= -\frac{2q(\eta)d\eta}{\pi} \frac{y(x-\eta)^2}{[(x-\eta)^2+y^2]^2} \\ d\tau_{xy} &= -\frac{2q(\eta)d\eta}{\pi} \frac{y^2(x-\eta)}{[(x-\eta)^2+y^2]^2} \end{aligned} \quad (2)$$

Taking vertical stress component as an example, we integrated Formula (2) in the limit equilibrium zone and the elastic zone, and we obtained the vertical stress components σ_{y1} , σ_{y2} generated by one-side abutment pressure distribution load at Point P, respectively:

$$\sigma_{y1} = -\frac{2\gamma H}{\pi} \int_0^{x_1} \frac{k\eta}{x_1} \frac{y^3 d\eta}{[(x-\eta)^2+y^2]^2} \quad (3)$$

$$\sigma_{y2} = -\frac{2\gamma H}{\pi} \int_{x_1}^{x_0} \left[\frac{(1-k)(\eta-x_1)}{x_0-x_1} + k \right] \frac{y^3 d\eta}{[(x-\eta)^2+y^2]^2} \quad (4)$$

We superposed the vertical stress components generated at Point P in the limit equilibrium zone and the elastic zone, and we obtained the vertical stress component generated by the abutment pressure distribution load on one side of the coal pillar at Point P:

$$\sigma_y = -\frac{2\gamma H}{\pi} \left\{ \int_0^{x_1} \frac{k\eta}{x_1} \frac{y^3 d\eta}{[(x-\eta)^2 + y^2]^2} + \int_{x_1}^{x_0} \left[\frac{(1-k)(\eta-x_1)}{x_0-x_1} + k \right] \frac{y^3 d\eta}{[(x-\eta)^2 + y^2]^2} \right\} \quad (5)$$

Similarly, we integrated the horizontal and shearing stress components in the limit equilibrium zone and the elastic zone, respectively, and the result is:

$$\begin{aligned} \sigma_x &= -\frac{2\gamma H}{\pi} \left\{ \int_0^{x_1} \frac{k\eta}{x_1} \frac{y(x-\eta)^2 d\eta}{[(x-\eta)^2 + y^2]^2} + \int_{x_1}^{x_0} \left[\frac{(1-k)(\eta-x_1)}{x_0-x_1} + k \right] \frac{y(x-\eta)^2 d\eta}{[(x-\eta)^2 + y^2]^2} \right\} \\ \tau_{xy} &= -\frac{2\gamma H}{\pi} \left\{ \int_0^{x_1} \frac{k\eta}{x_1} \frac{y^2(x-\eta) d\eta}{[(x-\eta)^2 + y^2]^2} + \int_{x_1}^{x_0} \left[\frac{(1-k)(\eta-x_1)}{x_0-x_1} + k \right] \frac{y^2(x-\eta) d\eta}{[(x-\eta)^2 + y^2]^2} \right\} \end{aligned} \quad (6)$$

According to the elastic-plastic theory, the ranges of the limit equilibrium zone x_1 and the elastic zone x_2 [26] are:

$$x_1 = \frac{m(1 - \sin \varphi)}{2f(1 + \sin \varphi)} \ln \left[\frac{k\gamma H(1 - \sin \varphi)}{2c_0 \cos \varphi} \right] \quad (7)$$

$$x_2 = x_0 - x_1 = \frac{m\beta}{2f} \ln k \quad (8)$$

where m is the mining height; c_0 is the coal cohesion; φ is the internal friction angle; f is the friction coefficient between the coal seam and the roof and floor; β is the lateral pressure coefficient. According to the geological data on the 33_{upper01} working face of Luwa Coal Mine, the parameters are taken as $m = 2.04$ m, $c_0 = 1.0$ MPa, $\varphi = 32^\circ$, $k = 3$, $\gamma = 25$ kN/m³, $H = 380$ m, $\beta = 1.5$. The results of Formulas (4) and (5) were brought into Formula (3). The stress distributions on the floor at different locations of special-shaped coal pillar are shown in Figures 7 and 8.

As shown in Figures 7 and 8, different sections of special-shaped coal pillars have stress concentration influence on the 3_{lower} coal seam. Section B-B only considers the stress concentration influence of the one-side abutment pressure of wide coal pillars on the floor; coal pillars in Section A-A are smaller than those in Section B-B and are more susceptible to the superposed abutment pressures on both sides, which have greater stress concentration influence on the floor. The vertical stresses of coal pillars on the floor are mainly concentrated underneath the coal pillars, with a large influence range. The one-side abutment pressures of coal pillars in Section A-A and Section B-B concentrated on the 3_{lower} coal seam are 8.75–13.48 MPa and 8.21–10.58 Mpa, respectively, so cross-coal pillar excavation in the 3_{lower} coal seam will be greatly influenced. Similarly, horizontal stresses are concentrated underneath the coal pillars, with a small influence range of stresses on the floor. With the increase in depth in the floor, the influence range gradually shifts towards the two edges of coal pillars. At 30 m underneath the coal seam, the concentrated horizontal stresses are only 0.88–2.26 Mpa and 0.44–1.38 Mpa, respectively, with little influence on the mining of the 3_{lower} coal seam. Shearing stresses are mainly concentrated on the two sides of coal pillars, with a wide influence range on the depth. The shearing stresses concentrated on the 3_{lower} coal seam are –3.84–3.84 Mpa and –2.78–2.82 Mpa, respectively. Thus, they have great influence on the inlet and outlet to the coal pillars in the cross-coal pillar excavation in the 3_{lower} coal seam.

To sum up, the 3_{lower} coal seam is mainly influenced by vertical stresses and shearing stresses generated by special-shaped coal pillars. Mining underneath the coal pillars is mainly influenced by vertical stresses and supplemented by shearing stresses; mining below the edges of coal pillars is influenced by the interaction of vertical stresses and shearing stresses. The horizontal stress concentration generated by special-shaped coal pillars on the floor has little influence on the mining of the 3_{lower} coal seam.

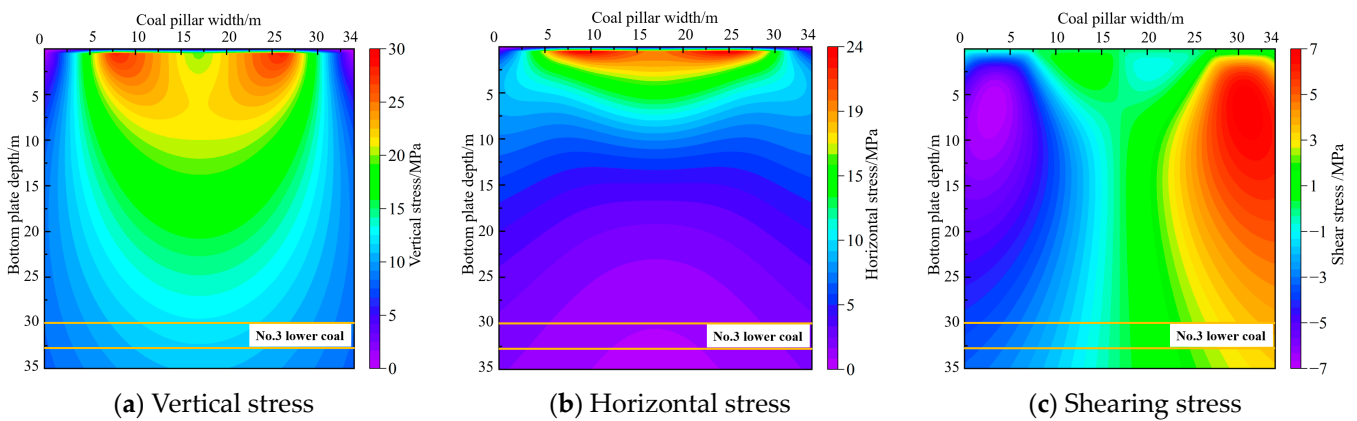


Figure 7. Stress distribution in Section A-A on the floor of special-shaped coal pillar.

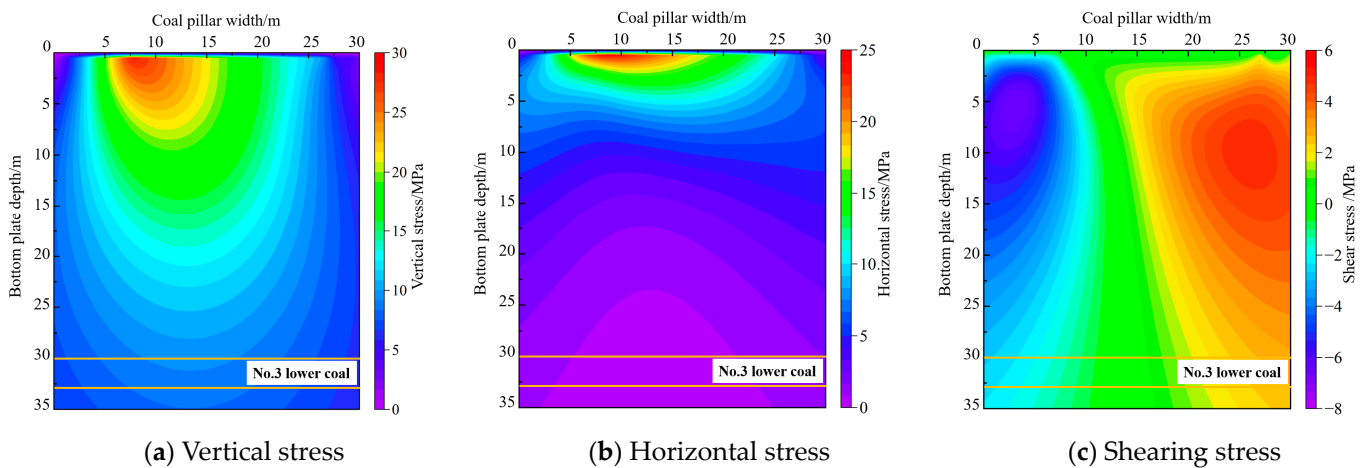


Figure 8. Stress distribution in Section B-B on one-side floor of special-shaped coal pillar.

3.2. Structural Characteristics of Lateral Overlying Strata in Fault Zones

After mining the working face in the fault-disturbed zone, the lateral main roof of the goaf was fractured, and the fractured position in the main roof of coal pillars protecting the roadway in the fault shifted to the depth of coal pillars. Influenced by lateral abutment pressure, the size of coal pillars protecting the roadway in the fault will affect fault activation and the instability of surrounding rock along the mining roadway in the fault-disturbed zone [27–29]. After the mining of lower working face in the fault, the goaf roof was fractured, swung and squeezed, forming a hinge structure, as shown in Figure 9. Based on the “voussoir beam” theory [30], the arc-shaped key block B was plastically hinged with the key block A on the coal pillar side and the key block C on the goaf side. Half load of the key block B was borne by the goaf gangue, and the other half was transferred to the coal pillars protecting the fault and the fault plane [31].

As shown in Figure 9, q is the unit area load on the main roof block; T is the horizontal extrusion pressure between the fault plane and Block A; h_2 is the thickness of Block A; h_1 is the thickness of the immediate roof; L_A is the width of Block A; L_B is the width of Block B; α is the turning sinking angle of Block B; θ is the dip angle of the fault; l is the width of coal pillars protecting the fault; s is the width of the roadway. In the mining of the lower part of coal pillars, the fault plane inclined to the working face side. According to the geometrical relationship, the conditions that the fault does not slip at the key stratum [32] are:

$$T \cos(90^\circ - \theta) \tan \varphi \geq T \sin(90^\circ - \theta) \quad (9)$$

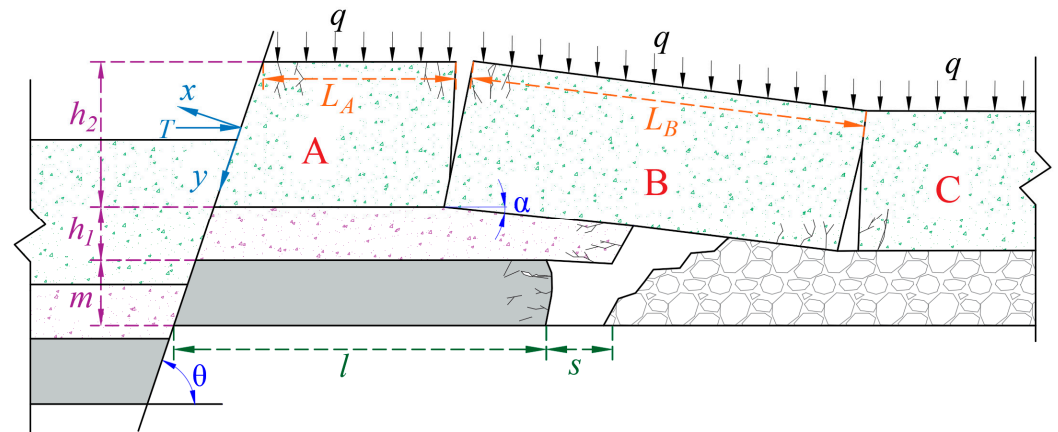


Figure 9. Structural model of lateral overlying strata in fault structure.

In general, $\varphi = 38\text{--}45^\circ$ [33]. We bring it into Formula (9). When $\theta > 45\text{--}52^\circ$, the frictional resistance generated by positive pressure perpendicular to the fault plane is greater than the slip thrust parallel to the fault plane. At this moment, the load generated by roof fracture, turning and sinking in the bottom wall of the goaf is shifted through the fault plane to the hanging wall of the fault as per a certain pressure coefficient. In the third mining area of Luwa Coal Mine, the dip angle of DF87 fault is $60\text{--}70^\circ$, which meets the condition that the fault does not slip at the key stratum. Therefore, the load transfer coefficient n ($0 \leq n \leq 1$, of which the value is related to intact coal pillars in the fault) is brought in, then the mining load Q_i transferred through the fault plane to the hanging wall is:

$$Q_1 = \frac{nqL_B \cos \alpha}{2} \tag{10}$$

The coal pillars protecting the fault are co-affected by the mining load that was not transferred from the fault plane to the hanging wall of the fault and the main roof of coal pillars, Block A and Block B. As a result, the load Q borne by the coal pillars is:

$$Q = \frac{(1-n)qL_B \cos \alpha}{2} + \gamma_1 h_1 \left(l + s - m \tan \theta - \frac{h_1 \tan \theta}{2} \right) + (\gamma_2 h_2 + q) \left(L_A + \frac{h_2 \tan \theta}{2} + \frac{L_B \cos \alpha}{2} \right) \tag{11}$$

where γ_1 is the main roof capacity; γ_2 is the immediate roof capacity.

The obtained load strength borne by the coal pillars of the fault is:

$$q_m = \frac{(1-n)qL_B \cos \alpha + \gamma_1 h_1 (2l + 2s - 2m \tan \theta - h_1 \tan \theta) + (\gamma_2 h_2 + q)(2L_A + h_2 \tan \theta + L_B \cos \alpha)}{2l} \tag{12}$$

According to the positional relationship between the working face layout and the fault panel, the width of coal pillars protecting the roadway on one side of the fault changes constantly, with which the load transfer coefficient changes. Based on the field geological production conditions and Formula (12), the influence law of load transfer coefficient and coal pillar width on the load strength borne by coal pillars of the fault is analyzed with the value assignment method, as shown in Figure 10.

As shown in Figure 10, the load strength borne by coal pillars of the fault is negatively correlated with load transfer coefficient and coal pillar width; load transfer coefficient is related to the integrity of coal pillars of the fault. As the coal rock near the fault zone is more fractured [34], the coal pillars of the fault are less integral, which influences the load transfer coefficient and the bearing capacity of coal pillars and will have negative effects on the stability of surrounding rocks along the mining roadway near the fault.

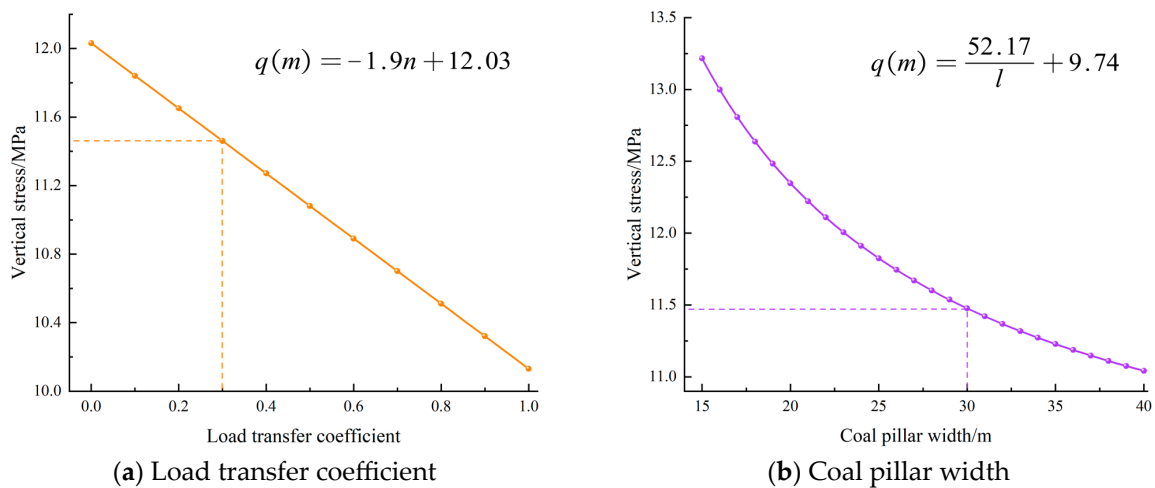


Figure 10. Influencing factors of load strength borne by coal pillars protecting the fault.

3.3. Numerical Calculation of Stress Field Superposed Effects

It is difficult to obtain through theoretical analysis the stress field distribution of coal pillars under the superposed effects of special-shaped coal pillars and fault disturbance. Therefore, numerical simulation is applied to make further analysis on the superposed effects of stress field. A numerical calculation model with a size of 300 m × 170 m × 70 m was established based on the actual geological conditions of Luwa Coal Mine. As shown in Figure 11, the average buried depth from the upper surface of the model to the ground surface is 380 m; the average unit weight of overlying strata is taken as 2.5 × 10⁴ Kn/m³. It can be calculated that the equivalent load exerted on the upper surface is about 9.5 MPa, and the gravity acceleration is 9.8 m/s². On the basis of existing studies, the Mohr–Coulomb constitutive model was adopted for numerical model [35,36]; the Double-Yield constitutive model was adopted for goaf gangue [37]; the model bottom was restrained by fixed displacement; the model periphery was restrained by horizontal displacement.

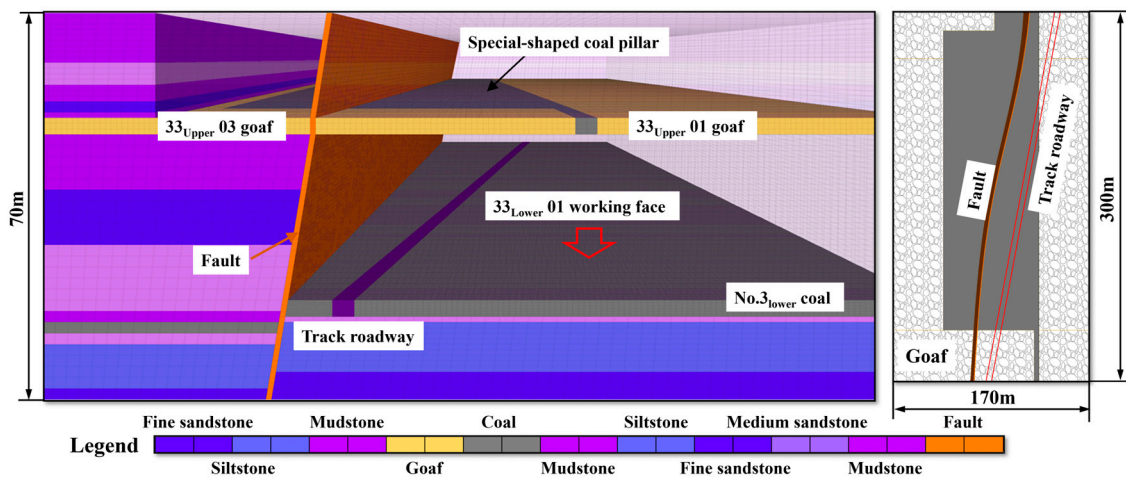


Figure 11. Numerical calculation model.

Table 1 shows the physical and mechanical parameters of coal mass in the numerical calculation model. The parameters were weakened to simulate the fault, and physical units were established in the fault zone (weak plane) in the model, in which the mechanical parameters are lower than the surrounding coal mass. Then, 1/20 of the corresponding mechanical parameters in the mudstone was selected, and half of the friction angles in the mudstone were taken as internal friction angles [38]. As Table 2.

Table 1. Physical and mechanical parameters in the rock mass.

Rock Stratum	Density /kg·m ⁻³	Bulk /Gpa	Shear /Gpa	Friction angle/°	Cohesion /MPa	Tensile /MPa
Mudstone	2580	3.3	2.1	36	1.5	2.3
Medium sandstone	2610	9.8	6.3	37	4.5	5.1
Mudstone	2580	3.3	2.1	36	1.5	2.3
Fine sandstone	2529	9.2	7.9	31	3.2	4.4
Mudstone	2580	3.3	2.1	36	1.5	2.3
No. 3 _{upper} coal	1480	1.5	1.1	30	1.2	0.9
Mudstone	2580	3.3	2.1	36	1.5	2.3
Fine sandstone	2529	9.2	7.9	31	3.2	4.4
Medium sandstone	2610	9.8	6.3	37	4.2	5.1
Mudstone	2580	3.3	2.1	36	1.5	2.3
No. 3 _{lower} coal	1480	1.5	1.1	30	1.2	0.9
Mudstone	2580	3.3	2.1	36	1.5	2.3
Siltstone	2590	9.8	8.1	36	3.2	6.7

Table 2. Physical and mechanical parameters in the fault.

Rock Stratum	Density /kg·m ⁻³	Bulk /Gpa	Shear /Gpa	Friction Angle/°	Cohesion /MPa	Tensile /MPa
Fault	129	0.165	0.105	18	0.075	0.115

For the determination of the physical and mechanical parameters of the goaf gangue, Jiang Lishuai, based on the stress–strain formula during the compaction process of fractured rock mass proposed by a foreign scholar Salamon, obtained the expression of compaction characteristics of rock mass in the caving zone [39].

$$\sigma = \frac{10.39\sigma_c^{1.042}}{b^{7.7}} \cdot \frac{\varepsilon}{1 - \frac{b}{b-1}\varepsilon} \quad (13)$$

where σ refers to vertical stress on the caving rock mass in the goaf; σ_c is the uniaxial compressive strength of the rock; b is the hulking coefficient of caving rock, which is taken as 1.33 in combination with the lithology of goaf roof [40]; ε is the strain of rock mass in the caving zone. According to Formula (13), the theoretical stress–strain solution on the gangue cover of the goaf is calculated as in Table 3.

Table 3. Theoretical stress–strain solution on the gangue cover of the goaf.

Strain	Stress/MPa	Strain	Stress/MPa	Strain	Stress/MPa	Strain	Stress/MPa
0	0	0.06	2.62	0.12	7.69	0.18	21.68
0.01	0.34	0.07	3.23	0.13	9.03	0.19	26.83
0.02	0.72	0.08	3.91	0.14	10.63	0.20	34.10
0.03	1.13	0.09	4.67	0.15	12.55	0.21	45.20
0.04	1.58	0.10	5.54	0.16	14.90	0.22	64.18
0.05	2.07	0.11	6.54	0.17	17.86	0.23	104.08

The Double-Yield constitutive model built in the Flac^{3D} numerical calculation software was applied to inverse the compaction characteristic of the goaf gangue. First, a small model was established to conduct the compression simulation experiment. Parameters such as goaf gangue density, bulk modulus, and friction angle were modified with the trial-and-error method. Then, the compaction stress–strain relationship of rock mass in the caving zone that better fits the theoretical solution [41] is obtained, as shown in Figure 12. The parameters of goaf gangue are shown in Table 4.

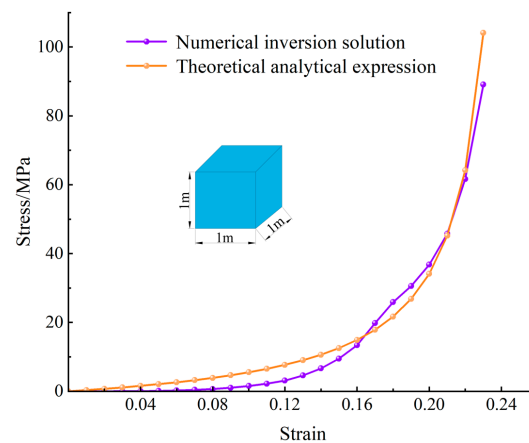


Figure 12. Mechanical properties inverted by double-yield model.

Table 4. Theoretical stress–strain solution on the gangue cover of the goaf.

Rock Stratum	Density/ $\text{kg}\cdot\text{m}^{-3}$	Bulk/ GPa	Shear/ Gpa	Friction Angle/ $^{\circ}$	Dilation Angle/ $^{\circ}$
Goaf gangue	1200	11.58	1.82	24	11

After the 33_{upper01} working face stimulating backstopping was balanced, the replacing 33_{upper03} working face was balanced after backstopping. The distribution of abutment pressures on the floor of special-shaped coal pillars and its effect on the lower part of the coal seam are shown in Figure 13.

As shown in Figure 13, after the mining in the working face of the 3_{upper} coal seam, the abutment pressures of special-shaped coal pillars were concentrated in the position near the coal pillar edge and the triangular area where the coal pillar size changed, representing a distribution of “three peaks and two ridges”. The “three peaks” refer to the triangular area where the coal pillar size changed, that is, the area with an orange mark in Figure 13a, of which the stress concentration peaks reached 42.14, 39.12 and 36.76 MPa, respectively. The two peaks on the left were formed by the superposed effects of high abutment pressures in the two parts. At the peak of 4 m on the right, the small coal pillar was seriously broken and released pressure influenced by the mining of working faces on both sides, causing similar stresses in this area with those at the two peaks on the left. The “two ridges” were caused by lateral high abutment pressures in the goaf on the coal pillars. On the goaf side of the 33_{upper01} working face, the peak of abutment pressures on the floor of coal pillars was 27.80 MPa; on the goaf side of the 33_{upper03} working face, the peak of abutment pressures on the floor of coal pillars was 24.82 MPa.

The DF87 positive fault segmented the stress concentration area of special-shaped coal pillars, forming a small distressed zone under the coal pillars. When the abutment pressures of special-shaped coal pillars were transferred to the lower slice, they were shifted and released to some degree. In the roadway excavation area on the hanging wall of the fault in the lower slice, the surrounding rock stress formed was 12.58–13.84 MPa, and the stress concentration coefficient was 1.26–1.38. When the roadway crossed special-shaped coal pillars, it went through the distressed zone under the goaf, the stress concentration area under special-shaped coal pillars, and the fault-disturbed zone. There was great difference in surrounding rock stresses, which would easily have adverse effects on the stability of the roadway.

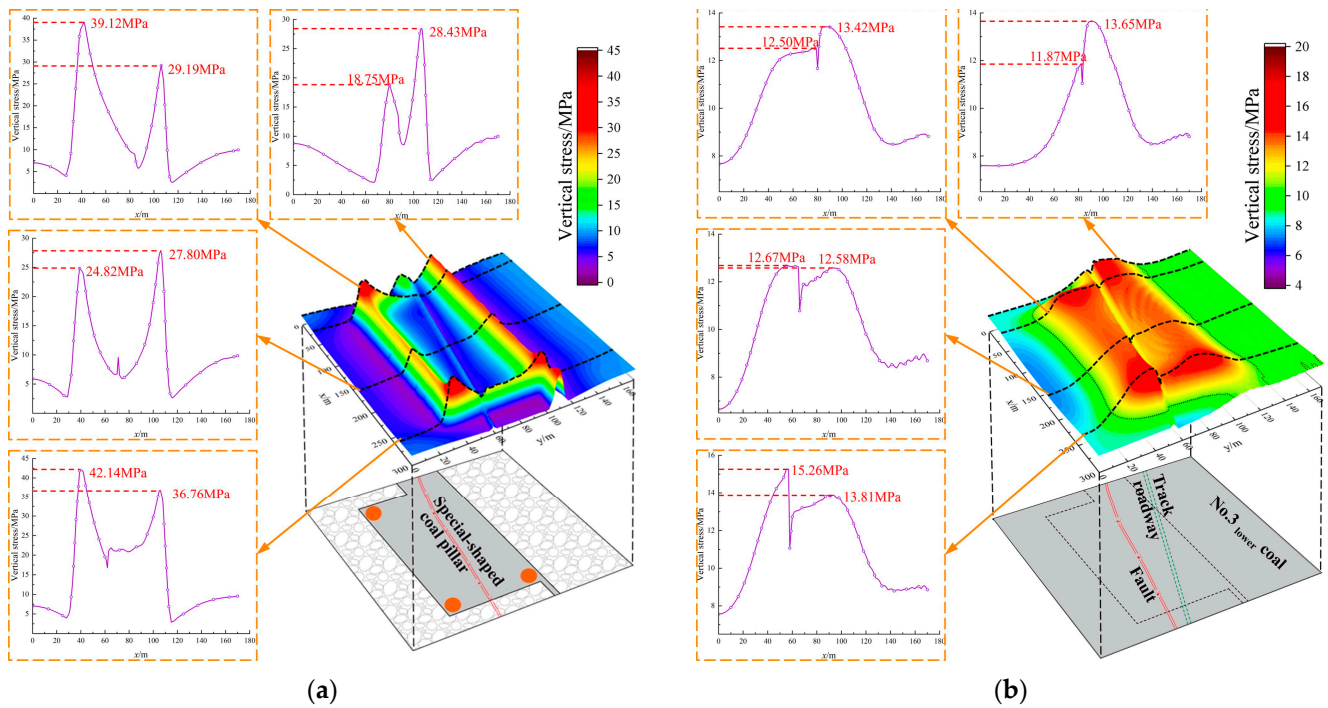


Figure 13. Superposed effects on the stress field. (a) Stress distribution on the floor of special-shaped coal pillars. (b) Stress distribution on 3_{lower} coal seam.

4. Stress Distribution Characteristics of Roadway Surrounding Rock in the Fault-Disturbed Zone under Special-Shaped Coal Pillars

4.1. Stress Distribution Characteristics of Surrounding Rock When the Mining Roadway Crosses Special-Shaped Coal Pillars

The 3_{lower} coal seam was influenced by the superposed effects of abutment pressures and fault disturbance of remaining special-shaped coal pillars after the mining of the 3_{upper} coal seam. The 33_{lower}01 track roadway represented different stress distribution characteristics in different sections of cross-excavation special-shaped coal pillars. To some degree, the fault curved the transfer of lateral overlying strata stresses. Therefore, the stresses on the roadway side of the fault were more concentrated than those on the roadway side of the working face along the mining roadway in the fault disturbed zone under special-shaped coal pillars. See Figure 14.

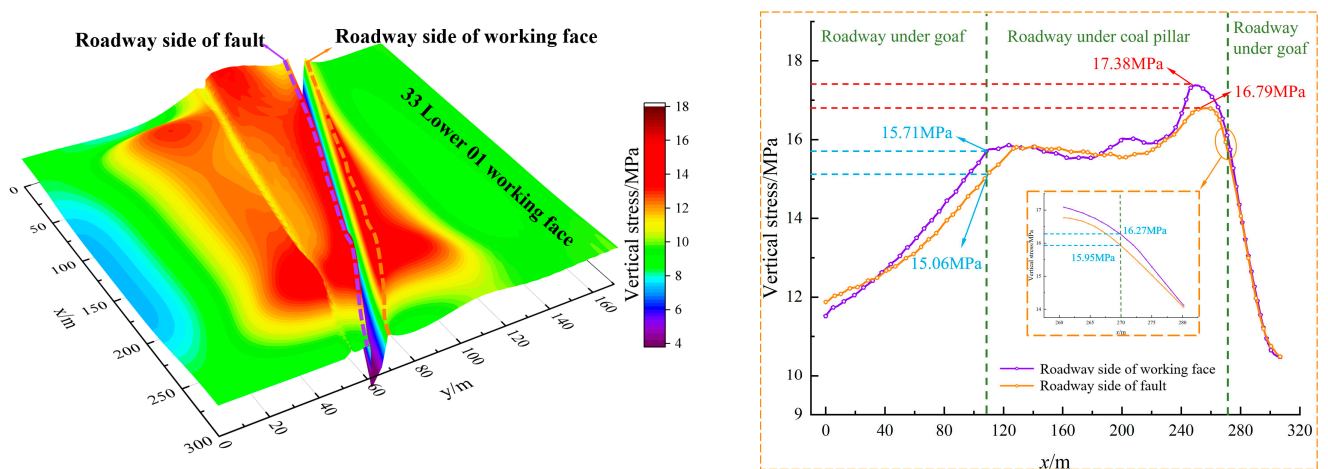


Figure 14. Stress distribution on surrounding rock when the mining roadway crosses special-shaped coal pillars.

As shown in Figure 14, when the roadway was under the goaf in the upper slice, the surrounding rock stress was low; the vertical stress excavated to the coal pillar edge gradually increased and reached 16.27 MPa when it entered the coal pillar; the stress concentration coefficient was about 1.51. When it moved about 12 m into the coal pillar, stress peaks emerged, and were asymmetrically distributed on the two roadway sidewalls; the peak value was 17.38 Mpa on the roadway side of fault and 16.79 Mpa on the roadway side of the working face; the stress concentration coefficients were 1.62 and 1.56, respectively; the increasing asymmetrical stress concentration had a great impact on the stability of the mining roadway in this stage. As the special-shaped coal pillars were large, the stress concentration was stable after the mining roadway excavated under the special-shaped coal pillars; the vertical stress was 15.71–16.02 Mpa; the stress concentration coefficient was about 1.46–1.49. When the mining roadway crossed and exited the special-shaped coal pillars, it would move from the stress-concentrated influence area of the coal pillar to the lower part of excavation and the distressed zone in the upper slice. As the roadway side of the working face reached beneath the distressed zone earlier than the roadway side of the fault, the stresses on the roadway side of the fault were more concentrated than those on the roadway side of the working face, with the stress concentration coefficients of 1.46 and 1.40, respectively. After exiting the coal pillars, the mining roadway arrived beneath the excavation and distressed zone in the upper slice, where the stress concentration coefficient gradually decreased from 1.40 to 1.07.

According to the spatial position relationship between special-shaped coal pillars and the mining roadway, the 33_{lower}01 track roadway can be divided into “lower section of goaf → the section crossing coal pillar edge → lower section of coal pillars → the section obliquely crossing coal pillar edge → lower section of goaf”, as shown in Figure 15. During the cross-excavation in the mining roadway, the superposed effects of special-shaped coal pillars and fault disturbance ranged from large to small as follows: the section crossing coal pillar edge > lower section of coal pillars > the section obliquely crossing coal pillar edge > lower section of goaf.

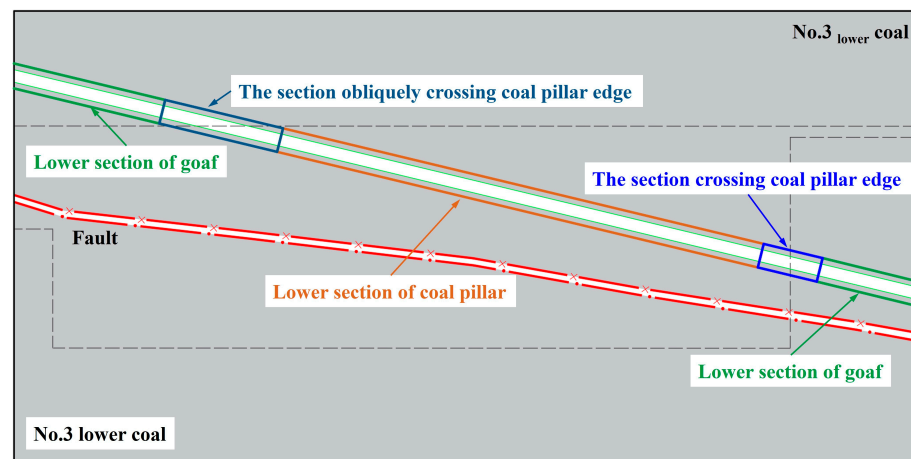


Figure 15. Sections of 33_{lower}01 track roadway.

4.2. Deviatoric Stress Distribution Characteristics on the Roadway Surrounding Rock

Based on the classical elastic-plastic theory and the rock mass mechanics theory, the stresses at a point in the rock mass are mainly spheric stress and deviatoric stress, of which deviatoric stress controls the plastic deformation and damage of the rock mass. If we suppose the three vertical principal stresses in the rock mass to be σ_i ($i = 1, 2, 3$), the stresses at the point in the rock mass should be [42]:

$$\sigma = \begin{pmatrix} \sigma_1 & 0 & 0 \\ 0 & \sigma_2 & 0 \\ 0 & 0 & \sigma_3 \end{pmatrix} = \begin{pmatrix} \sigma_m & 0 & 0 \\ 0 & \sigma_m & 0 \\ 0 & 0 & \sigma_m \end{pmatrix} + \begin{pmatrix} s_1 & 0 & 0 \\ 0 & s_2 & 0 \\ 0 & 0 & s_3 \end{pmatrix} \quad (14)$$

where σ_1 , σ_2 and σ_3 are, respectively, the maximum, median and minimum principal stresses of any hexahedron on the rock mass; s_1 , s_2 and s_3 are, respectively, the maximum, median and minimum deviatoric stresses; the relationship with spheric stress tensor is $s_i = \sigma_i - \sigma_m$; σ_m , which is a component of spheric stress tensor, and its relationship with principal stresses is $\sigma_m = (\sigma_1 + \sigma_2 + \sigma_3)/3$.

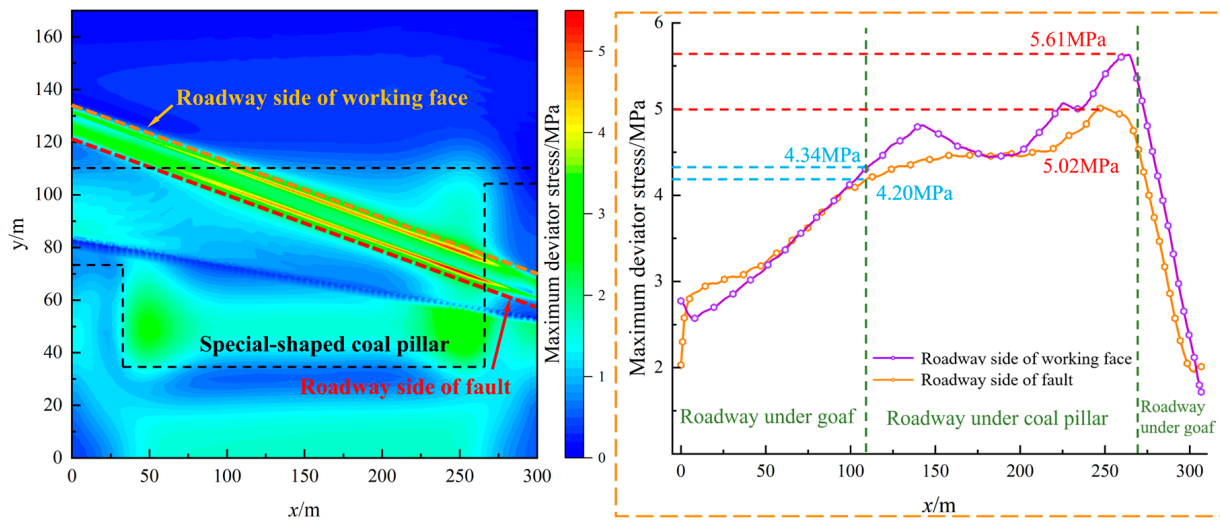
The deviatoric stress tensor plays a key role in the plastic deformation and damage of rock mass. It can be used to describe the deformation damage and stress state of an object and to judge the characteristics of deformation and failure along the mining roadway in the mining of the working face in the fault-disturbed zone under special-shaped coal pillars. In Formula (14), the relationship between the maximum deviatoric stress and principal stress is:

$$s_1 = \sigma_1 - \frac{1}{3}(\sigma_1 + \sigma_2 + \sigma_3) \quad (15)$$

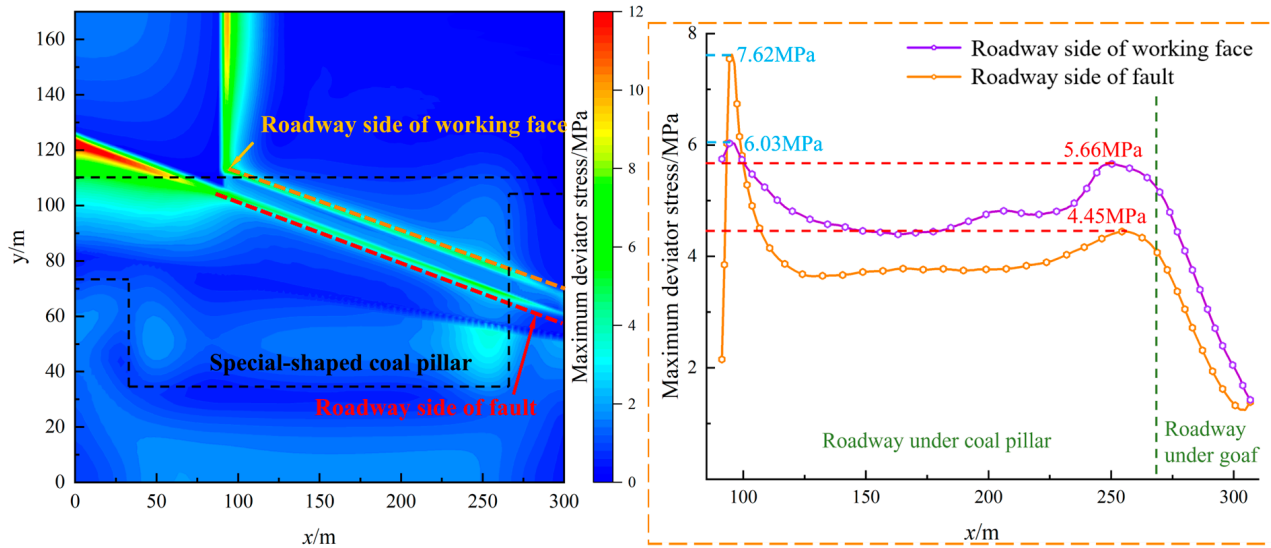
As the working face mining went through the process “lower section of goaf → the section obliquely crossing coal pillar edge → lower section of coal pillars → the section crossing coal pillar edge → lower section of goaf”, the distribution of maximum deviatoric stresses on the surrounding rock is shown in Figure 16.

As shown in Figure 16, under the superposed effects of special-shaped coal pillars and the fault, after the mining of the roadway, the deviatoric stresses were concentrated on the two sidewalls along the roadway under coal pillars and reached the maximum in the section crossing the coal pillar edge, where the deviatoric stresses were more concentrated on the roadway side of the fault. At this moment, the deviatoric stress peak was 5.61 MPa on the roadway side of the fault and 5.02 MPa on the roadway side of the working face; the peak on the roadway side of the fault was 11.7% higher than that on the roadway side of the working face. In the mining of the working face, influenced by advanced abutment pressures, the deviatoric stress in the front of the working face first increased and then decreased, and the deviatoric stress peak on the roadway side of the working face was greater than that on the roadway side of the fault. As it moved away from the area influenced by advanced abutment pressures, the deviatoric stresses decreased gradually until they were basically consistent with the deviatoric stress distribution in the non-mining stage.

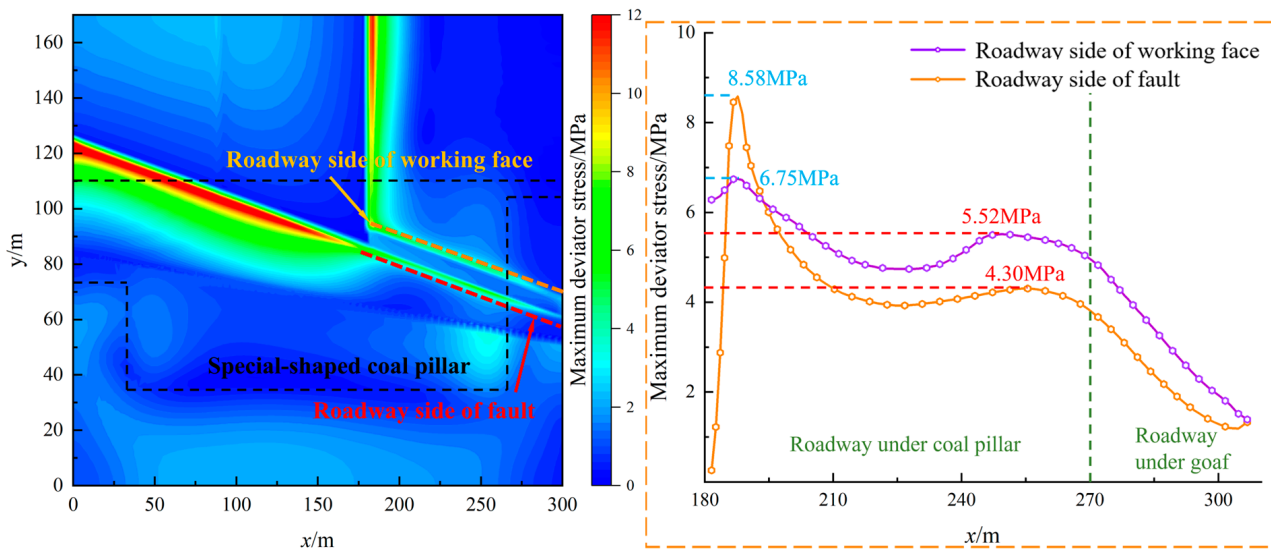
In the advanced segment in the section obliquely crossing the coal pillar edge (Figure 16b), the maximum deviatoric stress was 7.62 MPa on the roadway side of the working face and 6.03 MPa on the roadway side of the fault, which, respectively, increased by 81.4% and 38.9% compared with those in the non-mining stage. In the non-mining stage, deviatoric stresses are concentrated under the coal pillars. Therefore, when the mining face was mined below the coal pillars (Figure 16c), under advanced abutment pressures, the concentrated peaks of deviatoric stresses became higher: the deviatoric stress peak was 8.58 MPa on the roadway side of the working face, and 6.75 MPa on the roadway side of the fault, which, respectively, increased by 84.5% and 45.2% compared with those in the non-mining stage. When the mining face reached the section crossing the coal pillar edge (Figure 16d), the deviatoric stresses concentrated in front of the working face reached the maximum: the deviatoric stress was 9.13 MPa on the roadway side of the working face, and 7.66 MPa on the roadway side of the fault, which, respectively, increased by 97.6% and 41.3% compared with those in the non-mining stage. That the values are greater indicates that surrounding rock stresses change fast and are most influenced by the superposed effects of special-shaped coal pillars and the fault-disturbed zone. At this moment, it is susceptible to high stresses, which will easily lead to deformation and failure of roadway surrounding rock, and vice versa. It can be seen that during the mining of the 33_{lower}.01 working face, the superposed effects of special-shaped coal pillars and fault disturbance ranged from large to small as follows: the section crossing coal pillar edge > lower section of coal pillars > the section obliquely crossing coal pillar edge > lower section of goaf.



(a) Non-mining stage

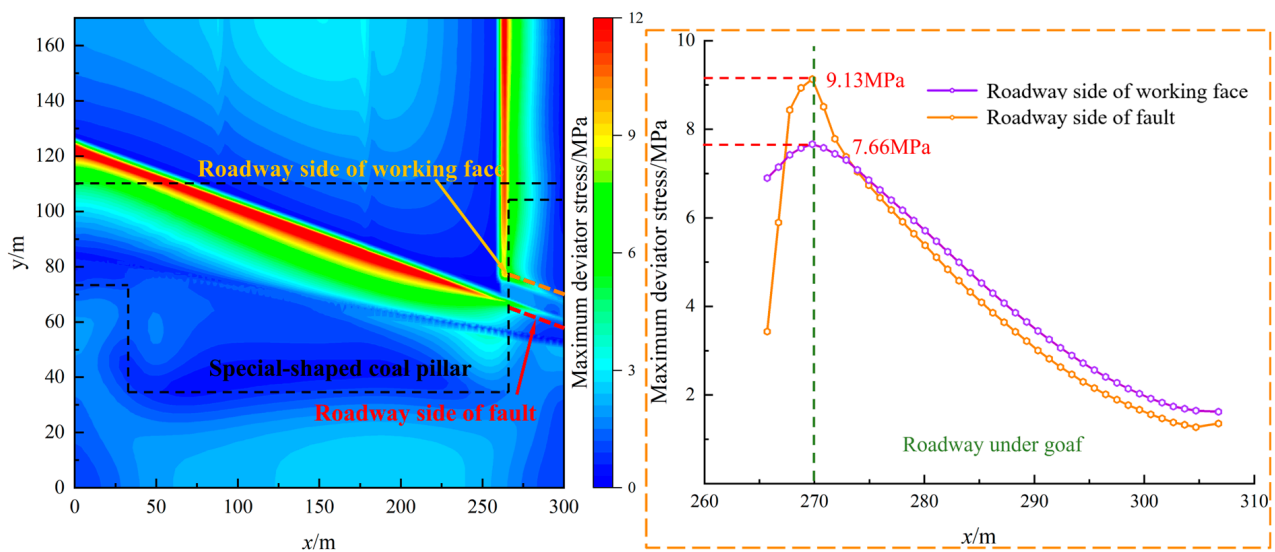


(b) The section obliquely crossing coal pillar edge



(c) Lower section of coal pillars

Figure 16. Cont.



(d) The section crossing coal pillar edge

Figure 16. Distribution of maximum deviatoric stresses in the mining of working face.

5. Discussion

According to the above field investigation, theoretical analysis, and numerical stimulation results, after the mining of the upper layered working face, the abutment pressure of the floor of the 3_{upper} coal seam exhibits a “three peaks and two ridges” distribution, resulting in the $3_{\text{lower}01}$ track roadway being influenced by the superposed effects of special-shaped coal pillars and fault disturbance in the whole service cycle. Because the fault blocked the transfer of some lateral overlying strata stresses, the stresses on the roadway side of the fault were more concentrated than those on the roadway side of the working face along the roadway in the fault-disturbed zone. The stresses were most influenced in the lower section crossing the coal pillar edge. After the mining roadway crossed the coal pillars, the stress concentration coefficient in the surrounding rock could reach 1.62. The results are basically consistent with the theoretical analysis. The high degree of stress concentration in the surrounding rock would lead to the failure and instability of surrounding rock along the roadway. In the mining of the working face, influenced by advanced abutment pressures, deviatoric stresses were concentrated in the advanced segment of the mining roadway, and more concentrated on the roadway side of the working face. Under high deviatoric stresses, the roadway sidewalls were easier to bulge and deform. The roof was influenced by shearing stresses, so that the supporting body was shorn off and fails, and the roof was separated, which would cause roof fall.

The stress distribution in small-sized coal pillars in this study is not yet clear, and the theoretical model on the impact mechanism and scope of fault disturbance lacks details. If the theoretical model is optimized, the theoretical analytical solution may be more in line with engineering practice. In the future, more relevant practices and research are needed to achieve safe and efficient mining of short-distance coal seams.

Comparing the existing research results, most of them only consider the effect of coal pillar or fault disturbance on the roadway layout and the stability of surrounding rocks [7–12,15], and propose the corresponding control technology. The mining conditions of the short-distance coal seams in Luwa Coal Mine are more special, and the existence of faults leads to irregular working face layout. The superimposed effects of the special-shaped coal pillars remaining in the upper seam and the fault disturbance result in a stress environment in the lower mining roadway that is quite different from normal conditions. Therefore, according to the superposed effects of special-shaped coal pillars and fault disturbance on the mining roadway, it is necessary to take some measures to adjust stress and use surrounding rock control technology to reinforce and support special

sections, in order to improve the stress field distribution of the roadway surrounding rock and ensure the stability of mining roadway in the service cycle. Next, we will propose the control technology of roadway surrounding rock and verify the rationality of the control technology of roadway surrounding rock through on-site monitoring.

6. Roadway Surrounding Rock Control Technology

6.1. Segmental Control Strategies

The fracture of coal mass near the fault zone may lead to fault activation, influenced by the disturbance of lateral high stresses, and even cause rockburst and other dynamic disasters. Therefore, the segmental control strategies of mining roadway stability in the fault-disturbed zone under special-shaped coal pillars is proposed as follows, based on theoretical analysis and numerical stimulation results, according to the pressure behavior characteristics along the mining roadway in the fault-disturbed zone under special-shaped coal pillars, as shown in Figure 17:

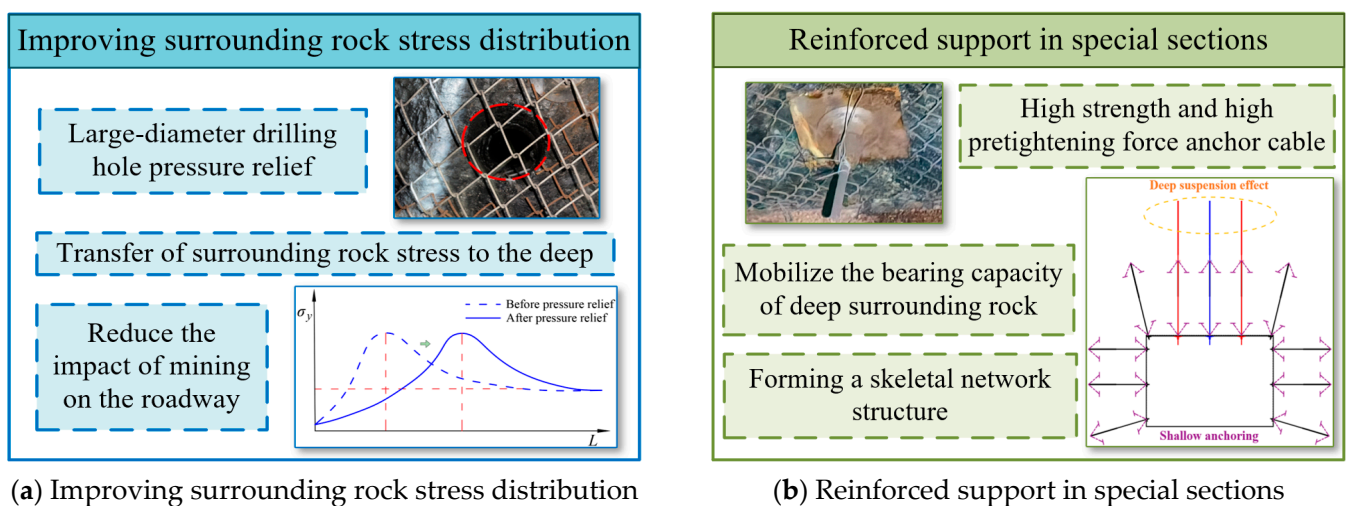


Figure 17. The segmented control strategies of mining roadway.

(1) Improving surrounding rock stress distribution

After the roadway was excavated, stresses were concentrated around the roadway. Under superposed effects of special-shaped coal pillars and fault disturbance, the stresses became more concentrated and the roadway surrounding rock remained in a high stress state [43]. The stress distribution on roadway surrounding rock can be improved by using large-diameter drilling hole pressure relief. Under high stresses, the coal mass surrounding the drilling hole was gradually fractured, forming a hole collapse zone and a plastic zone whose diameters were bigger than that of drilling hole. The elastic energy accumulated in the coal mass could be released, which transferred the high stresses in the roadway surrounding rock into the depth [44,45]. Thus, the superposed effects of special-shaped coal pillars and fault disturbance on the mining roadway were reduced.

(2) Reinforced support in special sections

In view of the influence of superposed effects of special-shaped coal pillars and fault disturbance on the roadway in the mining of working face, reinforced support is used for “the inlet to coal pillar” and “the outlet of coal pillar” with anchor cables of high strength, high pretightening force, and superior mechanical properties. On the one hand, reinforced support of anchor cables can connect the deep surrounding rock with the pretightening force bearing structure formed by rock bolt support. This will fully mobilize the bearing capacity of deep surrounding rock and realize the common bearing capacity of rock mass in a wider range [46]. On the other hand, the high pretightening force provides surrounding rock with compressive stress, which played a part in forming a skeletal network structure

with the compression stress area formed with rock bolts, keeping the overall stability of surrounding rock [47,48].

6.2. Segmental Control Technology

According to the segmental control approach to surrounding rock along the mining roadway in the fault-disturbed zone under special-shaped coal pillars, the segmental control technology of surrounding rock along the mining roadway in the fault-disturbed zone under special-shaped coal pillars is proposed. The segmental control technology of surrounding rock along the mining roadway on the site is shown in Figure 18.

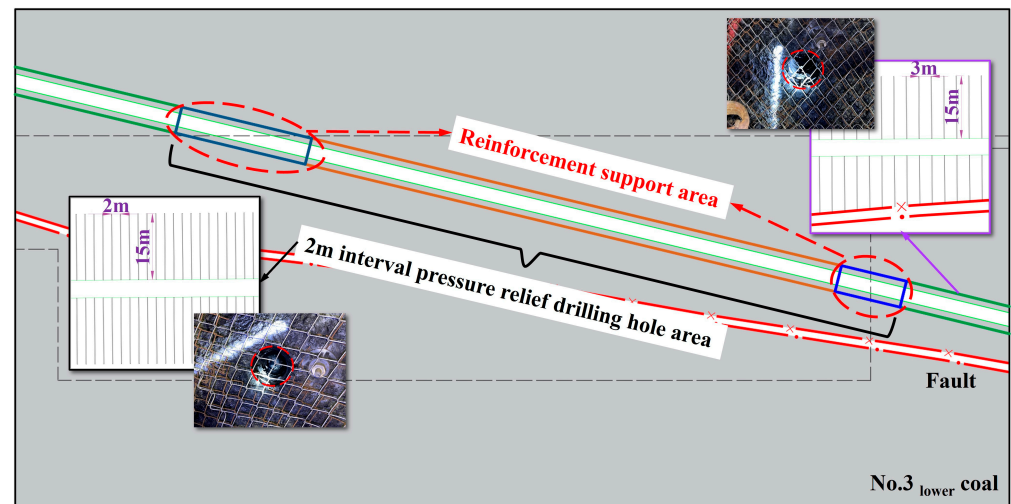


Figure 18. Segmental control technology of mining roadway.

(1) Large-diameter drilling hole pressure relief

On the two sidewalls on the track roadway of the 33_{lower}01 working face, a large-diameter (150 mm) drilling hole was used for pressure relief, and the roadway side of the working face was mined into a depth of 15 m. When the distance from the fault plane and the roadway was less than 15 m, the drilling depth into the roadway side of fault was the distance from the roadway sidewall to the fault plane. The hole was 1.2 m from the floor; the pitch of holes was 3 m, and it was 2 m in the fault-disturbed zone under special-shaped coal pillars. The drilling direction was perpendicular to the roadway sidewall and parallel to the coal seam.

(2) Reinforced support with anchor cables

The track roadway on 33_{lower}01 working face is jointly supported by anchor cables. The roof is supported by “rock bolt + anchor cable + metal mesh”. The rock bolt is in resin deformed steel bar, with a strength of No. 5 (A5) steel, a size of $\Phi 20 \times 2000$ mm, and a row spacing of 1000×1000 mm. The anchor cable is a $\Phi 17.8 \times 6000$ mm steel strand. One steel strand is arranged in each row, with a row-to-row distance of 3000 mm. The whole fault is covered by 10# iron wire diamond mesh of 5000×800 mm, and the mesh size is 75×75 mm. The sidewall is supported by “rock bolt + metal mesh”; the floor angles are supported by “inclined rock bolts”. The rock bolt is $\Phi 18 \times 1800$ mm of full-threaded FRP resin, with a row spacing of 1000×1000 mm, as shown in Figure 19. Red refers to reinforced support anchor cables. On either side of the center line on the roadway roof, there is a $\Phi 17.8 \times 6000$ mm reinforced support of 1×7 left-handed low-slack steel stranded anchor cable, with a pretightening force of not less than 250 KN and a spacing of 3000 mm.

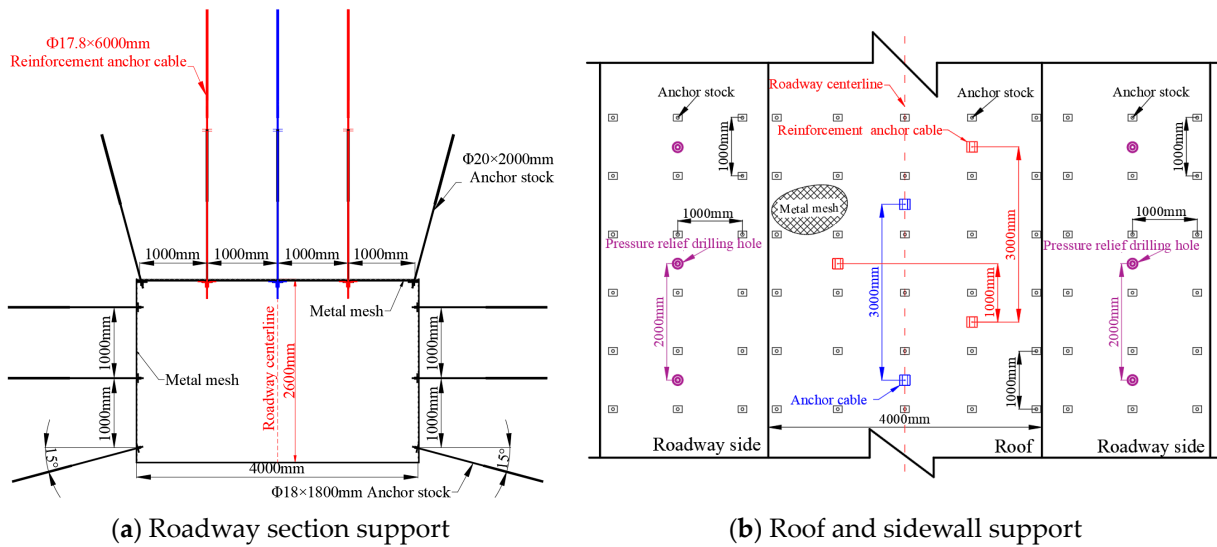


Figure 19. Reinforced support of 33_{lower}01 track roadway.

6.3. Evaluation of on-Site Applications

In order to verify the control effect of surrounding rock along the mining roadway in the fault-disturbed zone under special-shaped coal pillars, the cross-line detection method was adopted to monitor the surrounding rock deformation in 33_{lower}01 track roadway, as shown in Figures 20 and 21.

As shown in Figures 20 and 21, the mining roadway in the fault-disturbed zone under special-shaped coal pillars is stable overall. During the 50-day observation period, the deformation of roadway surrounding rock tended to be stable in about 35 days; the cumulative roof-to-floor convergence along the roadway in the lower section of coal pillars is 101.6 mm, and the cumulative convergence in the sidewall is 87.5 mm; the roof-to-floor cumulative convergence in the section crossing coal pillar edge is 124.1 mm, and the cumulative convergence in the sidewall is 99.8 mm; the convergence rates of the deformation of roadway roof and floor to the original sizes are 3.9% and 4.7%, respectively, which are overall controlled within 5%. The on-site control effect is shown in Figure 22. It can be seen that the improvement of stress distribution and reinforced support on the surrounding rock along the mining roadway effectively reduced the superposed influence of special-shaped coal pillars and fault disturbance on the mining roadway. Thus, effective control on surrounding rock along the mining roadway was realized.

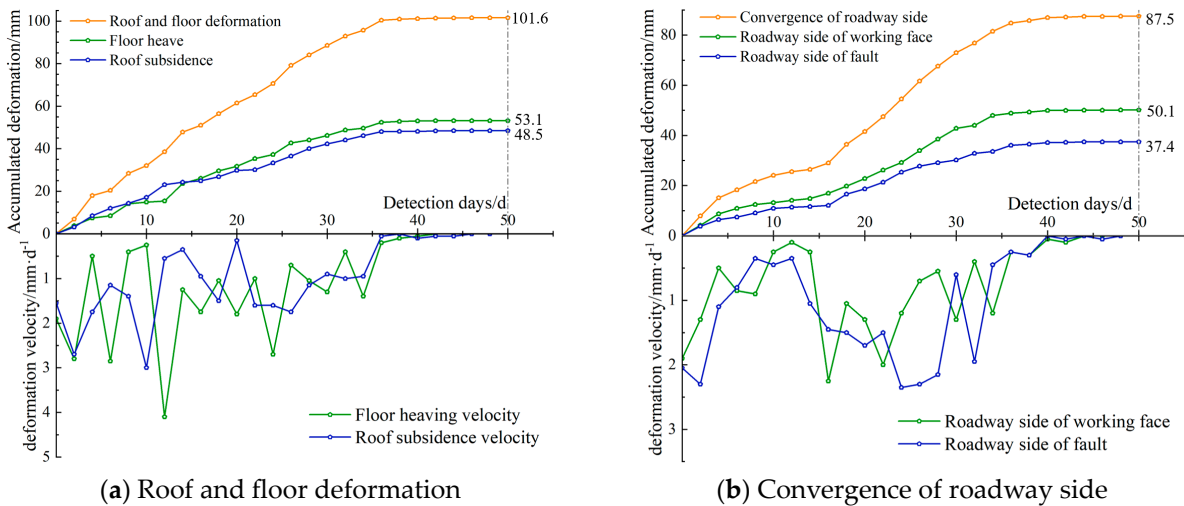


Figure 20. Roadway in the lower section of coal pillars.

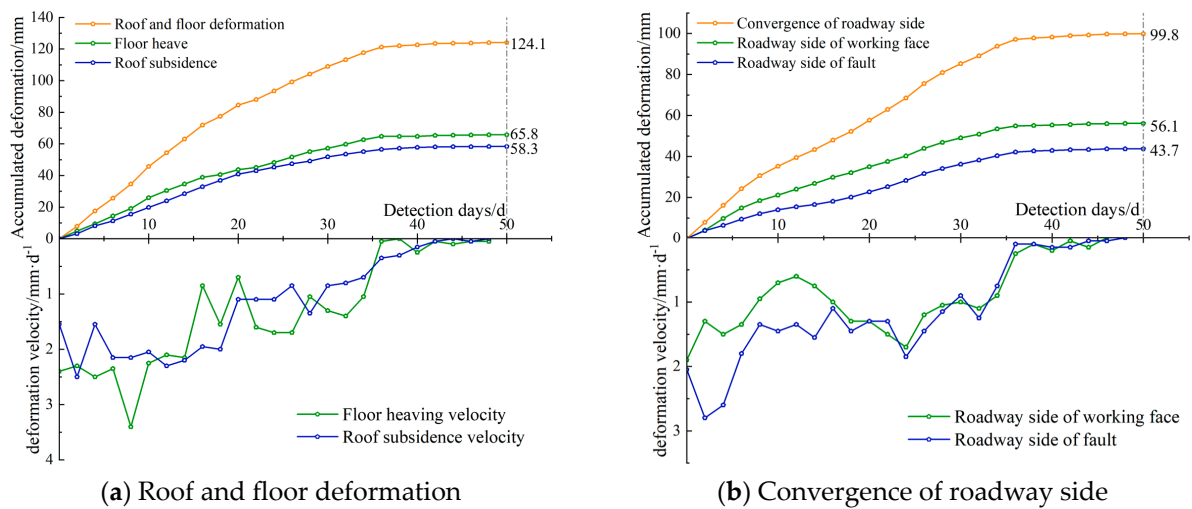


Figure 21. Roadway in the section crossing coal pillar edge.

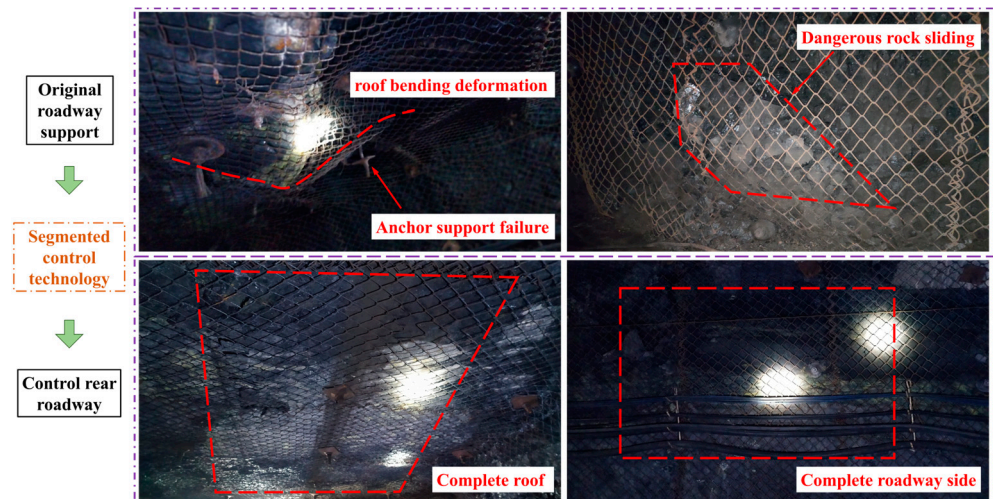


Figure 22. Control effects of surrounding rock in the 33_{lower}01 track roadway.

7. Conclusions

- (1) The effects of special-shaped coal pillars on 3_{lower} coal seams are dominated by vertical stresses and shearing stresses. The lower part of coal pillars is mainly disturbed by vertical stresses. The lower part of the special-shaped coal pillar edge will be influenced by the interaction of vertical stresses and shearing stresses. The stability of roadway surrounding rock in the fault-disturbed zone is closely related to the co-effects of lateral overlying strata structure on the fault side, overlying strata load, mining stresses, and the size of coal pillars protecting the fault.
- (2) The numerical simulation results show that the abutment pressures on the floor of special-shaped coal pillars represent a distribution of “three peaks and two ridges”. The positive fault segmented the area with concentrated stresses of special-shaped coal pillars, forming a small pressure relief zone. After the abutment pressures were transferred to the 3_{lower} coal seam, a concentrated area is generated in the 3_{lower} coal seam, with the stress concentration coefficient of about 1.26–1.38.
- (3) Based on the superimposed influence of special-shaped coal pillars and fault disturbance, the roadway was divided into the lower section of goaf, the section crossing coal pillar edge, the lower section of coal pillars, and the section obliquely crossing coal pillar edge. During the mining of the working face, under the influence of advanced support pressure, the degree of influence of the superposition of special-

shaped coal pillars and fault disturbances on the mining roadway further increases. The section crossing the coal pillar edge was the most influenced, and the maximum deviator stress is 9.13 MPa.

- (4) The segmental control approach to surrounding rock was proposed, which “improves the stress distribution on surrounding rock + reinforces support in special sections”. The joint control technology of large-diameter drilling hole pressure relief and special section anchor cable reinforcement support was adopted to conduct field practice. The monitoring result shows that the convergence rate of roadway surrounding rock was controlled within 5% overall, which effectively controlled the deformation of roadway surrounding rock.

Author Contributions: Conceptualization, C.L. and F.W.; methodology, C.L. and F.W.; software, C.L. and T.T.; validation, C.L., F.W. and Z.Z.; formal analysis, D.Z. and C.Z.; investigation, D.Z. and C.Z.; resources, F.W.; data curation, C.L. and X.Z.; writing—original draft preparation, C.L.; writing—review and editing, C.L., Z.Z. and F.W.; visualization, W.H. and T.T.; supervision, W.H.; project administration, F.W.; funding acquisition, F.W. All authors have read and agreed to the published version of the manuscript.

Funding: This research was funded by the National Natural Science Foundation of China (51974297), the Xuzhou Key R&D Plan (KC22283), the Graduate Innovation Program of China University of Mining and Technology (2023WLJCRCZL034).

Data Availability Statement: Data are contained within the article.

Conflicts of Interest: The authors declare no conflict of interest.

References

1. He, S.; Xie, S.; Song, B.; Zhou, D.; Sun, Y.; Han, S. Breaking laws and stability analysis of damage main roof in close distance hypogynous seams. *J. China Coal Soc.* **2016**, *41*, 2596–2605. [[CrossRef](#)]
2. Kang, H.; Lv, H.; Gao, F.; Meng, X.; Feng, Y. Understanding mechanisms of destressing mining-induced stresses using hydraulic fracturing. *Int. J. Coal Geol.* **2018**, *196*, 19–28. [[CrossRef](#)]
3. Zhu, W.; Xu, J.; Chen, L.; Li, Z.; Liu, W. Mechanism of disaster induced by dynamic instability of coal pillar group in room-and-pillar mining of shallow and close coal seams. *J. China Coal Soc.* **2019**, *44*, 358–366. [[CrossRef](#)]
4. Qin, K.; Wang, J.; Li, H.; Liu, W.; Bi, Z.; Kong, L. Study on abnormal mine pressure and mechanism of near—distance coal seam induced by concentrated coal pillar. *Coal Sci. Technol.* **2019**, *47*, 102–107. [[CrossRef](#)]
5. Zhao, H.; Cheng, H.; Ji, D.; Wang, T.; Wang, Y.; Jiang, C. Study of the mechanism and evolution law of unsymmetrical failure of the mining roadway in close distance coal seam. *Univ. Min. Technol.* **2021**, *50*, 1029–1040+1050.
6. Hu, S.; Xu, X.; Tian, S.; Zhang, B. Optimization of roadway location in lower coal seam from synergy mechanism of contiguous seam mining. *J. Min. Saf. Eng.* **2016**, *33*, 1008–1013. [[CrossRef](#)]
7. Li, C.; Wang, H.; Shi, Y. Study on disturbing influence of overlying remaining coal pillars on underlying coal seam mining. *Coal Sci. Technol.* **2020**, *48*, 232–239. [[CrossRef](#)]
8. Wang, F.; Shao, D.; Niu, T.; Dou, F. Progressive loading characteristics and accumulated damage mechanisms of shallow-buried coal pillars in withdrawal roadways with high-strength mining effect. *Chin. J. Rock Mech. Eng.* **2022**, *41*, 1148–1159. [[CrossRef](#)]
9. Wang, H.; Zhang, Y.; Pang, Y. Rational Layout of Roadway for Downward Cross-Pillar Mining in Close Distance Coal Seams. *J. Northeast. Univ.* **2023**, *44*, 100–109.
10. Du, J.; Huang, Q. Overburden structure evolution and coal pillar stability analysis with different offset distance of coal pillars in shallow multi-seam. *J. Min. Strat. Control. Eng.* **2022**, *4*, 16–24. [[CrossRef](#)]
11. Wang, F.; Liang, N.; Li, G.; Zhao, B. Failure evolution mechanism of coal pillar dams in complex stress environment. *J. Min. Saf. Eng.* **2019**, *36*, 1145–1152. [[CrossRef](#)]
12. Ji, H.; Ma, H.; Wang, J.; Zhang, Y.; Cao, H. Mining disturbance effect and mining arrangements analysis of near-fault mining in high tectonic stress region. *Saf Sci.* **2012**, *50*, 649–654. [[CrossRef](#)]
13. Duan, K.; Ji, Y.; Xu, N.; Wan, Z.; Wu, W. Excavation-induced fault instability: Possible causes and implications for seismicity. *Tunn. Undergr. Space Technol.* **2019**, *92*, 103041. [[CrossRef](#)]
14. Sainoki, A.; Mitri, H.S. Dynamic behaviour of mining-induced fault slip. *Int. J. Rock Mech. Min. Sci.* **2014**, *66*, 19–29. [[CrossRef](#)]
15. Feng, F.; Zhao, X.; Chen, S.; Li, H.; Yin, D.; Jiang, N.; Wang, F.; Sheng, S.; Yan, Z.; Zhang, X. A Design Method Forenergy-Releasing Supportsystem of Slabbing Rockburst Inhard Rock Subjected to Highstresses at Great Depth. Patent CN202111461703.0, 3 December 2021.
16. Chen, S.; Feng, F.; Li, X.; Wang, C.; Li, D.; Rostami, J.; Zhu, Q. Research progress and key issue of laboratory test and numerical-simulation for slabbing failure in hard rock under complex mining conditions. *J. China Univ. Min. Technol.* **2023**, *52*, 868–888.

17. Wang, F.; Xie, H.; Zhou, C.; Wang, Z.; Li, C. Combined effects of fault geometry and roadway cross-section shape on the collapse behaviors of twin roadways: An experimental investigation. *Tunn. Undergr. Space Technol.* **2023**, *137*, 105106. [[CrossRef](#)]
18. Huang, Q.; Du, J.; Chen, J.; He, Y. Coupling control on pillar stress concentration and surface cracks in shallow multi-seam mining. *Int. J. Min. Sci. Technol.* **2020**, *31*, 95–101. [[CrossRef](#)]
19. Jiang, Z.; Guo, W.; Xie, S. Coal Pillar Size Determination and Surrounding Rock Control for Gob-Side Entry Driving in Deep Soft Coal Seams. *Processes* **2023**, *11*, 2331. [[CrossRef](#)]
20. Wang, Q.; Feng, H.; Tang, P.; Peng, Y.; Li, C.; Jiang, L.; Mitri, H.S. Influence of Yield Pillar Width on Coal Mine Roadway Stability in Western China: A Case Study. *Processes* **2022**, *10*, 251. [[CrossRef](#)]
21. Das, A.J.; Mandal, P.K.; Paul, P.S.; Sinha, R.K. Generalised Analytical Models for the Strength of the Inclined as well as the Flat Coal Pillars using Rock Mass Failure Criterion. *Rock Mech. Rock Eng.* **2019**, *52*, 3921–3946. [[CrossRef](#)]
22. Li, S.; Zhou, L.; Luo, M.; Dong, H.; Qi, X. Strata behaviors analysis of stage coal pillar in Tong Xin mine caused by repeated mining. *J. Liaoning Tech. Univ. Nat. Sci.* **2015**, *34*, 661–667. [[CrossRef](#)]
23. Song, C.-H.; Lu, C.-P.; Zhang, X.-F.; Wang, C.; Xie, H.-D.; Yan, X.-Y.; Yang, H.-W. Moment Tensor Inversion and Stress Evolution of Coal Pillar Failure Mechanism. *Rock Mech. Rock Eng.* **2022**, *55*, 2371–2383. [[CrossRef](#)]
24. Li, H.; Gao, S.; Chen, D.; Xie, S.; Wu, Y.; Feng, S.; Jiang, Z.; Guo, F. Study on the Stability of Coal Pillars in a Gob-Side Two-Entry Arrangement of Different Layers in Fully Mechanized Caving and the Zonal Linkage Control of “Heteromorphic” Surrounding Rock. *Processes* **2023**, *11*, 1806. [[CrossRef](#)]
25. Qiang, S.; Jialiang, G.; Feng, Y.; Ruhong, B. Cooperative mining technology and strata control of close coal seams and overlying coal pillars. *Alex. Eng. J.* **2023**, *73*, 473–485. [[CrossRef](#)]
26. Wang, F.; Shang, J.; Zhao, B.; Cao, Q.; Niu, T. Strengthened anchor cable support mechanism and its parameter optimization design for roadway’s dynamic pressure section. *Univ. Min. Technol.* **2022**, *51*, 56–66. [[CrossRef](#)]
27. Alber, M.; Fritschen, R.; Bischoff, M.; Meier, T. Rock mechanical investigations of seismic events in a deep longwall coal mine. *Int. J. Rock Mech. Min. Sci.* **2009**, *46*, 408–420. [[CrossRef](#)]
28. Zhao, H.; Ma, F.; Xu, J.; Guo, J.; Yuan, G. Experimental investigations of fault reactivation induced by slope excavations in China. *Bull. Eng. Geol. Environ.* **2014**, *73*, 891–901. [[CrossRef](#)]
29. Cao, Y.; Zhang, J.; Yang, T.; Chu, H.; Zhang, X.; Zhang, T. Mechanism and Application of Prestressed Yielding Support for Large-Span Roadway in Multistress Concentration Areas. *Processes* **2023**, *11*, 1600. [[CrossRef](#)]
30. Qian, M.; Miao, X.; He, F. Analysis the key block of “masonry beam” structure in stope. *J. China Coal Soc.* **1994**, *6*, 557–563.
31. Yao, Q.; Wang, F.; Ma, S.; Zheng, C.; Li, J.; Xia, J.; Li, Y.; Luo, H.; Wu, C. Characteristics and control of strong underground pressure appear under irregular section normal fault roadway pillar. *J. Min. Saf. Eng.* **2022**, *39*, 1095–1107. [[CrossRef](#)]
32. Han, K.; Yu, Q.; Zhang, H.; Li, F. Mechanism of fault activation when mining on hanging-wall and foot-wall. *J. China Coal Soc.* **2020**, *45*, 1327–1335. [[CrossRef](#)]
33. Dai, J.; Jiang, J. Influence of mining sequence of hanging wall and foot wall on mining-induced stress of fault coal pillar. *J. Min. Saf. Eng.* **2016**, *33*, 35–41. [[CrossRef](#)]
34. Du, S.; Li, D.; Zhang, C.; Mao, D.; Ruan, B. Deformation and strength properties of completely decomposed granite in a fault zone. *Geophys. Geo-Energy Geo-Resour.* **2021**, *7*, 13. [[CrossRef](#)]
35. Liu, X.S.; Tan, Y.L.; Ning, J.G.; Lu, Y.W.; Gu, Q.H. Mechanical properties and damage constitutive model of coal in coal-rock combined body. *Int. J. Rock Mech. Min. Sci.* **2018**, *110*, 140–150. [[CrossRef](#)]
36. Wei, X.; Shahani, N.M.; Zheng, X.; Wang, J.; Wang, Y.; Chen, C.; Ren, Z. The Retention and Control Technology for Rock Beams in the Roof of the Roadway: A Case Study. *Processes* **2023**, *11*, 1593. [[CrossRef](#)]
37. Jin, Z.; Yang, Z.; Liu, G.; Li, F. Study on effect of residual coal pillar in coal seam group mining and surrounding rock control of cross-excavation roadway. *Coal Sci. Technol.* **2022**, *50*, 253–2336. [[CrossRef](#)]
38. Cai, S. Study and Application of the Interface and Weaken Method in FLAC3D Fault Simulation. Ph.D. Thesis, China University of Mining & Technology, Xuzhou, China, 2016. Available online: https://kns.cnki.net/kcms2/article/abstract?v=3uoqlhG8C475K0m_zrgu4lQARvep2SAkkyu7xrzFWukWlYlpgWWcEqx7YDBcgMfFkpWjGNF3t0nZX4PsIbgUAK7LHtn9UdFx&uniplatform=NZKPT (accessed on 21 July 2023).
39. Jiang, L.; Wu, Q.; Li, X.; Ding, N. Numerical simulation on coupling method between mining-induced stress and goaf compression. *J. China Coal Soc.* **2017**, *42*, 1951–1959. [[CrossRef](#)]
40. Zhang, C.; Bai, Q.; Zhu, C. A methodology for determining the size distribution of broken rock masses in longwall mining goaf. *Geo-Energy Geo-Resour.* **2022**, *8*, 113. [[CrossRef](#)]
41. Zhu, G.; Liu, B.; Dou, L.; Wu, Y.; Ding, Z. Numerical simulation for whole process of longwall mining on the basis of goaf compaction effect. *Univ. Min. Technol.* **2019**, *48*, 775–783. [[CrossRef](#)]
42. Deng, G.; Shao, S.; Chen, C.; She, F. A structural parameter reflecting coupling action between shear stress and spherical stress. *Rock Soil Mech.* **2012**, *33*, 2310–2314. [[CrossRef](#)]
43. Luo, Y.; Xu, K.; Huang, J.; Li, X.; Liu, T.; Qu, D.; Chen, P. Impact analysis of pressure-relief blasting on roadway stability in a deep mining area under high stress. *Tunn. Undergr. Space Technol.* **2021**, *110*, 103781. [[CrossRef](#)]
44. Xu, P.; Shao, J.; Fan, D.; Chang, J.; Zhang, N. Analysis of pressure relief effect of borehole in rock burst mine. *Energy Rep.* **2022**, *8*, 156–161. [[CrossRef](#)]

45. Wang, W.; Yuan, Y.; Ding, K.; Chen, Z.; Zhu, C.; Zhang, B.; Kofi, A.S.; Xia, Y.; Li, L. The Optimization of Segmented Reaming Parameters and the Analysis of the Pressure Relief Effect in Impacted Coal Seams. *Processes* **2023**, *11*, 1235. [[CrossRef](#)]
46. Zhang, W.; Zhao, T.-B.; Zhang, X.-T. Stability analysis and deformation control method of swelling soft rock roadway adjacent to chambers. *Géoméch. Geophys. Geo-Energy Geo. Resour.* **2023**, *9*, 91. [[CrossRef](#)]
47. Šňupárek, R.; Konečný, P. Stability of roadways in coalmines alias rock mechanics in practice. *J. Rock Mech. Geotech. Eng.* **2010**, *2*, 281–288. [[CrossRef](#)]
48. Fangtian, W.; Cun, Z.; Shuaifeng, W.; Xiaogang, Z.; Shenghua, G. Whole section anchor–grouting reinforcement technology and its application in underground roadways with loose and fractured surrounding rock. *Tunn. Undergr. Space Technol.* **2016**, *51*, 133–143. [[CrossRef](#)]

Disclaimer/Publisher’s Note: The statements, opinions and data contained in all publications are solely those of the individual author(s) and contributor(s) and not of MDPI and/or the editor(s). MDPI and/or the editor(s) disclaim responsibility for any injury to people or property resulting from any ideas, methods, instructions or products referred to in the content.